EUROPEAN ORGANIZATION FOR NUCLEAR RESEARCH

CERN-PPE 91-105
2 July 1991

Improved Measurements of Electroweak Parameters from Z Decays into Fermion Pairs

The ALEPH Collaboration*

Abstract

The properties of the Z resonance are measured on the basis of 190,000 Z decays into fermion pairs collected with the ALEPH detector at LEP. Assuming lepton universality, $M_{\mathrm{Z}} = (91.182 \pm 0.009_{\mathrm{exp}} \pm 0.020_{\mathrm{LEP}})$ GeV, $\Gamma_{\mathrm{Z}} = (2484 \pm 17)$ MeV, $\sigma^0_{\mathrm{had}} = (41.44 \pm 0.36)$ nb, and $\Gamma_{\mathrm{had}}/\Gamma_{\ell\ell} = 21.00 \pm 0.20$. The corresponding number of light neutrino species is 2.97 ± 0.07. The forward-backward asymmetry in leptonic decays is used to determine the ratio of vector to axial-vector coupling constants of leptons: $g^2_{\mathrm{V}}(M^2_{\mathrm{Z}})/g^2_{\mathrm{A}}(M^2_{\mathrm{Z}}) = 0.0072 \pm 0.0027$. Combining these results with ALEPH results on quark charge and $b\bar{b}$ asymmetries, and τ polarization, $\sin^2\theta_{\mathrm{W}}(M^2_{\mathrm{Z}}) = 0.2312 \pm 0.0018$. In the context of the Minimal Standard Model, limits are placed on the top-quark mass.

(Submitted to Zeitschrift für Physik C)

*See the following pages for the list of authors.

The ALEPH Collaboration

D. Decamp, B. Deschizeaux, C. Goy, J.-P. Lees, M.-N. Minard

Laboratoire de Physique des Particules (LAPP), IN^{2}P^3-CNRS, 74019 Annecy-le-Vieux Cedex, France

R. Alemany, J.M. Crespo, M. Delfino, E. Fernandez, V. Gaitan, Ll. Garrido, Ll.M. Mir, A. Pacheco

Laboratorio de Fisica de Altas Energias, Universidad Autonoma de Barcelona, 08193 Bellaterra (Barcelona), Spain[8]

M.G. Catanesi, D. Creanza, M. de Palma, A. Farilla, G. Iaselli[1], G. Maggi, M. Maggi, S. Natali, S. Nuzzo, M. Quattromini, A. Ranieri, G. Raso, F. Romano, F. Ruggieri, G. Selvaggi, L. Silvestris, P. Tempesta, G. Zito

INFN Sezione di Bari e Dipartimento di Fisica dell' Università, 70126 Bari, Italy

Y. Gao, H. Hu[21], D. Huang, X. Huang, J. Lin, J. Lou, C. Qiao[21], T. Ruan[21], T. Wang, Y. Xie, D. Xu, R. Xu, J. Zhang, W. Zhao

Institute of High-Energy Physics, Academia Sinica, Beijing, The People's Republic of China[9]

W.B. Atwood[2], L.A.T. Bauerdick, F. Bird, E. Blucher, G. Bonvicini, F. Bossi, J. Boudreau, D. Brown, T.H. Burnett[3], H. Drevermann, R.W. Forty, C. Grab, R. Hagelberg, S. Haywood, J. Hilgart, B. Jost, M. Kasemann, J. Knobloch, A. Lacourt, E. Lançon, I. Lehraus, T. Lohse, A. Lusiani, A. Marchioro, M. Martinez, P. Mato, S. Menary, A. Minten, A. Miotto, R. Miquel, H.-G. Moser, J. Nash, P. Palazzi, F. Ranjard, G. Redlinger, A. Roth, J. Rothberg[3], H. Rotscheidt, M. Saich, R. St.Denis, D. Schlatter, M. Takashima, M. Talby[4], W. Tejessy, H. Wachsmuth, S. Wasserbaech, S. Wheeler, W. Wiedenmann, W. Witzeling, J. Wotschack

European Laboratory for Particle Physics (CERN), 1211 Geneva 23, Switzerland

Z. Ajaltouni, M. Bardadin-Otwinowska, R. El Fellous, A. Falvard, P. Gay, J. Harvey, P. Henrard, J. Jousset, B. Michel, J-C. Montret, D. Pallin, P. Perret, J. Proriol, F. Prulhière, G. Stimpfl

Laboratoire de Physique Corpusculaire, Université Blaise Pascal, IN^{2}P^3-CNRS, Clermont-Ferrand, 63177 Aubière, France

J.D. Hansen, J.R. Hansen, P.H. Hansen, R. Møllerud, B.S. Nilsson

Niels Bohr Institute, 2100 Copenhagen, Denmark[10]

I. Efthymiopoulos, E. Simopoulou, A. Vayaki

Nuclear Research Center Demokritos (NRCD), Athens, Greece

J. Badier, A. Blondel, G. Bonneaud, J. Bourotte, F. Braems, J.C. Brient, G. Fouque, A. Gamess, R. Guirlet, S. Orteu, A. Rosowsky, A. Rougé, M. Rumpf, R. Tanaka, H. Videau

Laboratoire de Physique Nucléaire et des Hautes Energies, Ecole Polytechnique, IN^2P^3-CNRS, 91128 Palaiseau Cedex, France

D.J. Candlin, E. Veitch

Department of Physics, University of Edinburgh, Edinburgh EH9 3JZ, United Kingdom[11]

G. Parrini

Dipartimento di Fisica, Università di Firenze, INFN Sezione di Firenze, 50125 Firenze, Italy

M. Corden, C. Georgiopoulos, M. Ikeda, J. Lannutti, D. Levinthal,[16] M. Mermikides, L. Sawyer

Supercomputer Computations Research Institute and Dept. of Physics, Florida State University,
Tallahassee, FL 32306, USA [13,14,15]

A. Antonelli, R. Baldini, G. Bencivenni, G. Bologna,[5] P. Campana, G. Capon, F. Cerutti, V. Chiarella, B. D'Ettorre-Piazzoli,[6] G. Felici, P. Laurelli, G. Mannocchi,[6] F. Murtas, G.P. Murtas, G. Nicoletti, L. Passalacqua, M. Pepe-Altarelli, P. Picchi,[5] P. Zografou

Laboratori Nazionali dell'INFN (LNF-INFN), 00044 Frascati, Italy

B. Altoon, O. Boyle, A.W. Halley, I. ten Have, J.L. Hearns, J.G. Lynch, W.T. Morton, C. Raine, J.M. Scarr, K. Smith, A.S. Thompson, R.M. Turnbull

Department of Physics and Astronomy, University of Glasgow, Glasgow G12 8QQ, United Kingdom[11]

B. Brandl, O. Braun, R. Geiges, C. Geweniger, P. Hanke, V. Hepp, E.E. Kluge, Y. Maumary, A. Putzer, B. Rensch, A. Stahl, K. Tittel, M. Wunsch

Institut für Hochenergiephysik, Universität Heidelberg, 6900 Heidelberg, Fed. Rep. of Germany[17]

A.T. Belk, R. Beuselinck, D.M. Binnie, W. Cameron, M. Cattaneo, P.J. Dornan,[1] S. Dugeay, A.M. Greene, J.F. Hassard, N.M. Lieske, S.J. Patton, D.G. Payne, M.J. Phillips, J.K. Sedgbeer, G. Taylor, I.R. Tomalin, A.G. Wright

Department of Physics, Imperial College, London SW7 2BZ, United Kingdom[11]

P. Girtler, D. Kuhn, G. Rudolph

Institut für Experimentalphysik, Universität Innsbruck, 6020 Innsbruck, Austria[19]

C.K. Bowdery,[1] T.J. Brodbeck, A.J. Finch, F. Foster, G. Hughes, N.R. Keemer, M. Nuttall, A. Patel, B.S. Rowlingson, T. Sloan, S.W. Snow, E.P. Whelan

Department of Physics, University of Lancaster, Lancaster LA1 4YB, United Kingdom[11]

T. Barczewski, K. Kleinknecht, J. Raab, B. Renk, S. Roehn, H.-G. Sander, M. Schmelling, H. Schmidt, F. Steeg, S.M. Walther, B. Wolf

Institut für Physik, Universität Mainz, 6500 Mainz, Fed. Rep. of Germany[17]

J-P. Albanese, J-J. Aubert, C. Benchouk, V. Bernard, A. Bonissent, D. Courvoisier, F. Etienne, S. Papalexiou, P. Payre, B. Pietrzyk, Z. Qian

Centre de Physique des Particules, Faculté des Sciences de Luminy, IN²P³-CNRS, 13288 Marseille, France

H. Becker, W. Blum, P. Cattaneo, G. Cowan, B. Dehning, H. Dietl, F. Dydak[26], M. Fernandez-Bosman, T. Hansl-Kozanecka,[22] A. Jahn, W. Kozanecki,[2,23] E. Lange, J. Lauber, G. Lütjens, G. Lutz, W. Männer, Y. Pan, R. Richter, J. Schröder, A.S. Schwarz, R. Settles, U. Stierlin, J. Thomas, G. Wolf

Max-Planck-Institut für Physik und Astrophysik, Werner-Heisenberg-Institut für Physik, 8000 München, Fed. Rep. of Germany[17]

V. Bertin, J. Boucrot, O. Callot, X. Chen, A. Cordier, M. Davier, G. Ganis, J.-F. Grivaz, Ph. Heusse, P. Janot, D.W. Kim,[20] F. Le Diberder, J. Lefrançois,[1] A.-M. Lutz, J.-J. Veillet, I. Videau, Z. Zhang, F. Zomer

Laboratoire de l'Accélérateur Linéaire, Université de Paris-Sud, IN²P³-CNRS, 91405 Orsay Cedex, France

D. Abbaneo, S.R. Amendolia, G. Bagliesi, G. Batignani, L. Bosisio, U. Bottigli, C. Bradaschia, M. Carpinelli, M.A. Ciocci, R. Dell'Orso, I. Ferrante, F. Fidecaro, L. Foà, E. Focardi, F. Forti, A. Giassi, M.A. Giorgi, F. Ligabue, E.B. Mannelli, P.S. Marrocchesi, A. Messineo, L. Moneta, F. Palla, G. Sanguinetti, J. Steinberger, R. Tenchini, G. Tonelli, G. Triggiani, C. Vannini, A. Venturi, P.G. Verdini, J. Walsh

Dipartimento di Fisica dell'Università, INFN Sezione di Pisa, e Scuola Normale Superiore, 56010 Pisa, Italy

J.M. Carter, M.G. Green,[1] P.V. March, T. Medcalf, I.S. Quazi, J.A. Strong, R.M. Thomas, L.R. West, T. Wildish

Department of Physics, Royal Holloway & Bedford New College, University of London, Surrey TW20 OEX, United Kingdom[11]

D.R. Botterill, R.W. Clifft, T.R. Edgecock, M. Edwards, S.M. Fisher, T.J. Jones, P.R. Norton, D.P. Salmon, J.C. Thompson

Particle Physics Dept., Rutherford Appleton Laboratory, Chilton, Didcot, OXON OX11 OQX, United Kingdom[11]

B. Bloch-Devaux, P. Colas, C. Klopfenstein, E. Locci, S. Loucatos, E. Monnier, P. Perez, J.A. Perlas, F. Perrier, J. Rander, J.-F. Renardy, A. Roussarie, J.-P. Schuller, J. Schwindling, B. Vallage

Département de Physique des Particules Elémentaires, CEN-Saclay, 91191 Gif-sur-Yvette Cedex, France[18]

J.G. Ashman, C.N. Booth, C. Buttar, R. Carney, S. Cartwright, F. Combley, M. Dinsdale, M. Dogru, F. Hatfield, J. Martin, D. Parker, P. Reeves, L.F. Thompson

Department of Physics, University of Sheffield, Sheffield S3 7RH, United Kingdom[11]

E. Barberio, S. Brandt, H. Burkhardt[1], C. Grupen, H. Meinhard, L. Mirabito, U. Schäfer, H. Seywerd

Fachbereich Physik, Universität Siegen, 5900 Siegen, Fed. Rep. of Germany[17]

G. Apollinari, G. Giannini, B. Gobbo, F. Liello, F. Ragusa[25], L. Rolandi, U. Stiegler

Dipartimento di Fisica, Università di Trieste e INFN Sezione di Trieste, 34127 Trieste, Italy

L. Bellantoni, X. Chen, D. Cinabro, J.S. Conway, D.F. Cowen[24], Z. Feng, D.P.S. Ferguson, Y.S. Gao, J. Grahl, J.L. Harton, J.E. Jacobsen, R.C. Jared[7], R.P. Johnson, B.W. LeClaire, Y.B. Pan, J.R. Pater, Y. Saadi, V. Sharma, Z.H. Shi, Y.H. Tang, A.M. Walsh, J.A. Wear[27], F.V. Weber, M.H. Whitney, Sau Lan Wu, G. Zobernig

Department of Physics, University of Wisconsin, Madison, WI 53706, USA[12]

This paper is dedicated to Emilio Picasso for his contributions as LEP Project Leader

---

[1]Now at CERN.
[2]Permanent adddress: SLAC, Stanford, CA 94309, USA.
[3]Permanent address: University of Washington, Seattle, WA 98195, USA.
[4]Also Centre de Physique des Particules, Faculté des Sciences, Marseille, France
[5]Also Istituto di Fisica Generale, Università di Torino, Torino, Italy.
[6]Also Istituto di Cosmo-Geofisica del C.N.R., Torino, Italy.
[7]Permanent address: LBL, Berkeley, CA 94720, USA.
[8]Supported by CAICYT, Spain.
[9]Supported by the National Science Foundation of China.
[10]Supported by the Danish Natural Science Research Council.
[11]Supported by the UK Science and Engineering Research Council.
[12]Supported by the US Department of Energy, contract DE-AC02-76ER00881.
[13]Supported by the US Department of Energy, contract DE-FG05-87ER40319.
[14]Supported by the NSF, contract PHY-8451274.
[15]Supported by the US Department of Energy, contract DE-FC0S-85ER250000.
[16]Supported by SLOAN fellowship, contract BR 2703.
[17]Supported by the Bundesministerium für Forschung und Technologie, Fed. Rep. of Germany.
[18]Supported by the Institut de Recherche Fondamentale du C.E.A..
[19]Supported by Fonds zur Förderung der wissenschaftlichen Forschung, Austria.
[20]Supported by the Korean Science and Engineering Foundation and Ministry of Education.
[21]Supported by the World Laboratory.
[22]On leave of absence from MIT, Cambridge, MA 02139, USA.
[23]Supported by Alexander von Humboldt Fellowship, Germany.
[24]Now at California Institute of Technology, Pasadena, CA 91125, USA.
[25]Now at Dipartimento di Fisica, Università di Milano, Milano, Italy.
[26]Also at CERN, PPE Division, 1211 Geneva 23, Switzerland.
[27]Now at University of California, Santa Cruz, CA 95064, USA.

1 Introduction

Measurements of cross sections and angular distributions for Z decay to fermion pairs place significant constraints on parameters of the Standard Model and allow tests of the consistency of the model.

In this paper, improved measurements of the parameters of the Z resonance based on 8.0 pb^{-1} of data collected with the ALEPH detector at LEP during 1989 and 1990 at and near the Z mass are presented. The data include 165,000 hadronic and 25,000 leptonic Z decays, and correspond to a sample three times larger than that of our previous analysis [1]. In addition to reduced statistical errors, improved analysis methods have led to substantially reduced systematic errors.

The ALEPH detector [2] and the techniques used to select different types of events [1] have been described elsewhere. Here, significant changes since the previous work and the additional systematic studies which have been done are discussed. The precision of the luminosity measurement is described in a separate paper [3], and is not addressed here.

2 Hadronic Event Selection

Hadronic events are selected with two independent methods, as described in Ref. [1]. One of these methods is based entirely on charged tracks, while the other depends on energy deposition in the electromagnetic (ECAL) and hadronic (HCAL) calorimeters. The track-based selection requires at least 5 charged tracks in the time-projection chamber (TPC), ALEPH's main charged-particle tracking chamber, and a charged-track energy sum (assuming pion masses) greater than 10% of the centre-of-mass energy. The calorimeter-based selection requires that the combined ECAL and HCAL energy exceeds 20% of the centre-of-mass energy. In addition, the minimum energy deposit in the ECAL must be either 7 GeV in the barrel or 1.5 GeV in each endcap. A time requirement of ± 100 ns with respect to the beam crossing, measured on ECAL signals, removes the bulk of cosmic-ray background. Additional requirements are imposed to suppress the background from lepton pairs [1].

For both selections, the background from leptonic decays of the Z is estimated from Monte Carlo. The two-photon background is measured with the data by exploiting the different centre-of-mass energy dependence of the two-photon background and hadronic decays of the Z. The trigger inefficiency is measured to be less than 0.03% by comparing two independent triggers, one based on ECAL energy, and the other based on hits in the Inner Tracking Chamber (ITC) in conjunction with hits in the HCAL.

The dominant systematic error in the track-based selection is a result of the requirement that the sum of the charged-track energies exceeds 10% of the centre-of-mass energy. The size of this systematic error is estimated from the effect of a shift of $0.01\sqrt{s}$ in the charged-energy distribution, corresponding to the observed shift between the data and the Monte Carlo simulation (see Fig. 1). The resulting uncertainty in the selection efficiency is 0.24%. As a check on this systematic error, the measured resonant cross section for events failing the charged energy requirement is compared with the Monte Carlo prediction. Resonant and nonresonant cross sections are separated with the technique already used to extract the two-photon background ($\sigma_{\gamma\gamma} = (118 \pm 23)$ pb corresponding to (0.39 ± 0.07)% of the peak hadronic cross section). In Fig. 1, the results of this measurement are plotted with the observed charged-energy distribution and the Monte Carlo prediction for $q\overline{q}$ events; the Monte Carlo distribution is normalized to the data for events with $E_{\rm CH} > 0.1\sqrt{s}$. The difference between the measured resonant cross section and the Monte Carlo prediction for events with $E_{\rm CH} < 0.1\sqrt{s}$ is (0.15 ± 0.17)%, which is consistent with the quoted systematic error. Combining all other systematic errors, including uncertainties in background contributions, the

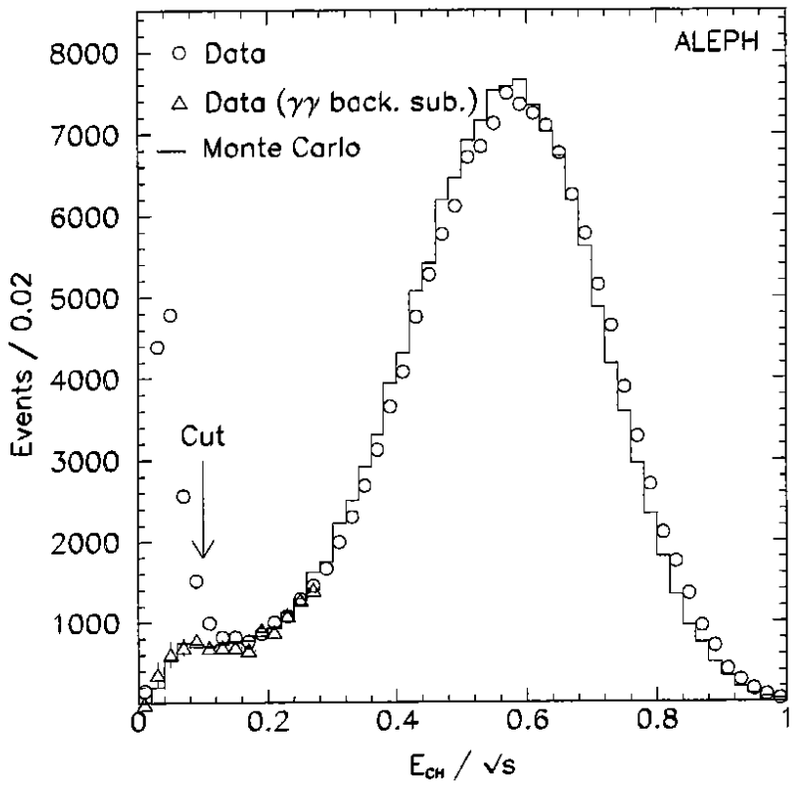

Figure 1: Charged-track energy sum per event for data (circles) and Monte Carlo (solid histogram). The triangles represent measured numbers of resonant events after the subtraction of two-photon background (see text). The Monte Carlo is normalized to the data for $E_{\rm CH}/\sqrt{s} > 0.1$.

systematic error in the track-based selection is 0.26% at $\sqrt{s} = M_{\rm Z}$.

The calorimeter-based selection has a larger efficiency than the track-based selection, and has a correspondingly smaller systematic uncertainty related to the selection requirements. The dominant systematic error comes instead from background in the $q\bar{q}$ sample. In particular, $\tau^+\tau^-$ events represent $(0.62 \pm 0.15)\%$ of the selected event sample. The remaining background comes from e^+e^- events, two-photon interactions, and cosmic rays, corresponding to (33 ± 12) pb, (70 ± 25) pb, and (26 ± 5) events/pb^{-1}, respectively. These numbers are given as percentages of the peak cross section in Table 1. The total systematic error of this selection is about 0.2% at $\sqrt{s} = M_{\rm Z}$.

Details of the two selections are summarized in Table 1. The error quoted for selection efficiency includes the statistical error from the Monte Carlo; the uncertainties in background subtractions are listed separately.

All of the events not common to both samples (about 4% of the events) have been scanned visually for evidence of detector or data-acquisition problems. An additional systematic error of 0.04% is assigned to account for the few problems which have been observed; these problems were related to a malfunction in the readout electronics of the TPC.

Since the systematic errors of the two selections are largely independent, the measured cross sections are averaged and an overall systematic error of 0.2% at $\sqrt{s} = M_{\rm Z}$ is quoted. As a check on the systematic error, the ratio of cross sections measured with the two selections is plotted as a function of energy (Fig. 2); the large correlation between the event samples is taken into account in the errors. A fit to these ratios yields $\sigma_{\rm cal}/\sigma_{\rm track} = 1.0023 \pm 0.0004$, which is consistent with the

Table 1: Hadronic Event Selections. The number of events corresponds to data at all centre-of-mass energies, while efficiencies, backgrounds, and systematic errors are quoted at the peak.

	Charged Track Selection	Calorimeter Selection
Events	166,158	169,993
Selection Efficiency (%)	97.4 ± 0.24	99.1 ± 0.09
Backgrounds:		
e^+e^- (%)	0	0.11 ± 0.04
$\tau^+\tau^-$ (%)	0.26 ± 0.03	0.62 ± 0.15
Cosmic-ray (%)	0	0.08 ± 0.02
Two-photon (%)	0.39 ± 0.07	0.23 ± 0.08
Total Sys. Error ($\sqrt{s} = M_Z$) (%)	0.26	0.20

quoted systematic errors.

3 Leptonic Event Selection

The leptonic branching ratios have been determined using procedures similar to those described in [1]. The leptonic branching fractions are measured separately for each type of lepton pair, and for all lepton pairs in common, without any attempt to distinguish among them. The comparison of this common-lepton sample with the separate lepton samples allows checks on the systematic biases of the event selection requirements. As will be discussed, the e^+e^- and $\mu^+\mu^-$ selections have been modified with respect to [1] to increase the acceptance for events with a radiated photon, thereby reducing systematic uncertainties in event selection efficiency. Improved understanding of backgrounds and efficiency also results in reduced systematic errors for the $\tau^+\tau^-$ and common-lepton $\ell^+\ell^-$ channels.

The theoretical treatment of the t-channel contribution to the e^+e^- and common-lepton samples is also improved with respect to [1]. A new program called ALIBABA [4], which allows a calculation of Bhabha scattering including $O(\alpha^2)$ initial-state radiation, is now available. The program can calculate the full s-channel, t-channel, and interference term, the s-channel alone, or the t-channel alone. Throughout this paper, the sum of the t-channel and the interference term is referred to as the t-channel contribution to the cross section. The results of ALIBABA have a reported accuracy of approximately 0.5% of the total cross section [4]. Corrections are necessary to make the results of ALIBABA, a semi-analytical program which gives results as functions of the polar angles and energies of the outgoing electron and positron, applicable to the experimental acceptance. Including the error in these corrections, the total systematic error in the t-channel subtraction is 2% of the pure t-channel part (not including s-t interference) of the subtraction. At the peak ($\sqrt{s} = M_Z$), the t-channel contribution is 12.2% of the total cross section in the angular range in which $Z \to e^+e^-(\gamma)$ events are selected. In addition, the sensitivity of the t-channel contribution to uncertainties in the Z mass and width is about 1% of the pure t-channel part of the cross section at the peak and smaller away from the peak. As a check of the t-channel subtraction procedure, a fit to the complete cross section (including t-channel and interference) has been done using the program MIBA [5]. This program, like ALIBABA, includes complete $O(\alpha)$ and leading log $O(\alpha^2)$ QED corrections with soft-photon exponentiation. The hadron and electron lineshapes have been fit simultaneously with and without t-channel subtraction. The results of the two methods agree to better than 0.1%; the results presented here are based on the t-channel subtraction method.

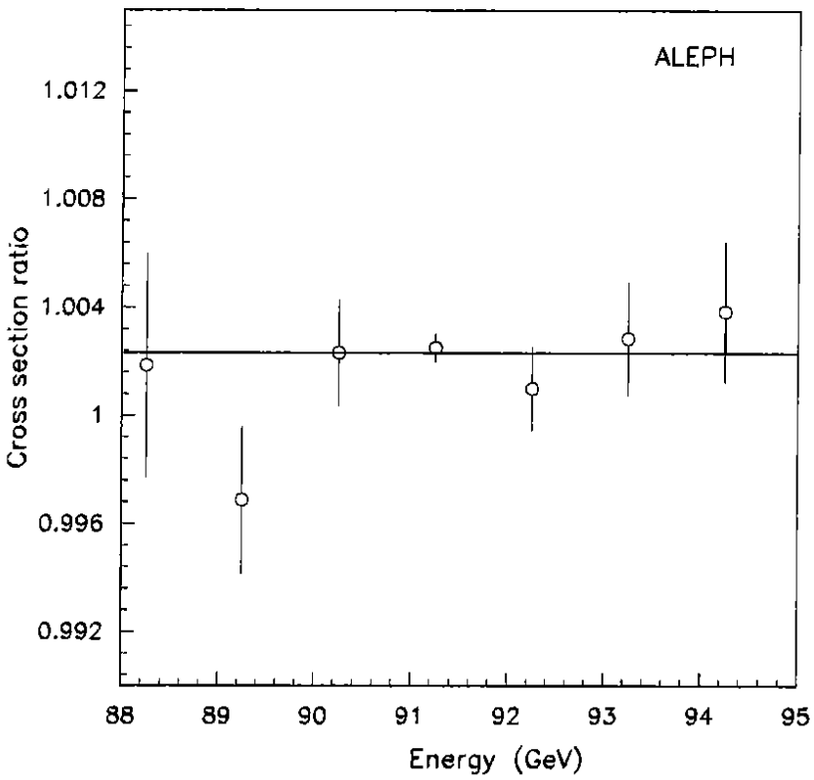

Figure 2: Ratio of cross section from calorimeter-based hadronic event selection to that of the charged-track based selection. The errors account for the correlation between the two event samples.

The forward-backward asymmetries $A_{\rm FB}(s)$ at each centre-of-mass energy are extracted from a fit to the angular distribution with the function [6]

$$\frac{d\sigma}{d\cos\theta^*} = C(1+\cos^2\theta^* + \frac{8}{3}A_{\rm FB}\cos\theta^*)F(\cos\theta^*) \tag{1}$$

using a maximum-likelihood method. C is a normalization constant and $F(\cos\theta^*)$ describes the effect of the t-channel exchange which is relevant only for the e^+e^- channel. The scattering angle, θ^*, between the incoming e^- and the outgoing fermion is defined as

$$\cos\theta^* = \sin\frac{1}{2}(\theta^+ + \theta^-)/\sin\frac{1}{2}(\theta^+ - \theta^-), \tag{2}$$

where θ^- and θ^+ are the polar angles of the vector sum of the track momenta[1] in the hemispheres corresponding to the outgoing fermion and antifermion, respectively. This variable preserves the true angular distribution in the e^+e^- centre-of-mass when hard collinear radiation takes place from the initial state.

Details of the lepton-pair selections are summarized in Table 2. A first series of requirements, which is common to all of the lepton-pair channels, is applied to eliminate hadronic events, as well as to suppress background from beam-gas, two-photon, and cosmic-ray events. These initial requirements are the following:

- Only tracks with 4 or more points measured in the TPC, which originate from the beam crossing within ± 10 cm along the beam direction and $\pm d_0$ in the transverse plane, are considered; these tracks are referred to as good. Two d_0 requirements are used: a more restrictive one ($d_0 = 2$ cm) and a less restrictive one ($d_0 = 5$ cm).

- The event is required to have either 2 and only 2 good tracks which pass the loose d_0 requirement or 3 to 8 good tracks which satisfy the restrictive d_0 requirement.

- The event is divided into two hemispheres by a plane perpendicular to the thrust axis. There must be at least one good track in each hemisphere.

- At least one good track with $d_0 < 2$ cm must have a reconstructed momentum greater than 3 GeV.

- Events with more than 4 tracks are rejected if any track has an angle greater than 31.8° with respect to the vector sum of the track momenta in the same hemisphere.

- The acollinearity, η_{acol}, defined as 180° minus the angle between the vector sum of the track momenta[2] in each hemisphere, must be smaller than 20°.

The multiplicity requirement makes the acceptance sensitive to inefficiencies in charged-track finding. This effect has been studied with a sample of e^+e^- pairs which were selected solely on the basis of calorimetric information. An inefficiency of $(0.25\pm0.10)\%$ in addition to the $(0.69\pm0.06)\%$ predicted by the Monte Carlo has been observed, and is corrected for in the analyses below; this inefficiency is the result of the TPC readout problem mentioned in the previous section.

In 1990, an additional charged electromagnetic trigger with a threshold of 0.2 GeV was implemented, improving the redundancy of the trigger. The trigger inefficiency is less than 0.15% for all lepton channels, and is known with an accuracy better than 0.05%.

[1] For the $e^+e^-(\gamma)$ final states, $\cos\theta^*$ is calculated from the two highest momentum tracks only.

[2] For the $e^+e^-(\gamma)$ final states, the acollinearity is calculated from the two highest momentum tracks only.

Table 2: Lepton-Pair Selections. The number of selected events corresponds to data at all centre-of-mass energies, while selection efficiencies, background, and systematic errors are quoted at the peak.

	e^+e^-	$\mu^+\mu^-$	$\tau^+\tau^-$	$\ell^+\ell^-$
Selected Events	6,947	6,691	6,260	24,757
Angular Range ($\cos\theta^*$)	$(-0.9, 0.7)$	$(-0.9, 0.9)$	$(-0.9, 0.9)$	$(-0.9, 0.9)$
Selection Efficiency (%)[3]	98.8 ± 0.3	98.4 ± 0.5	86.4 ± 0.8	98.3 ± 0.2
Overall Efficiency(%)	71.4 ± 0.4	83.1 ± 0.5	72.9 ± 0.8	83.0 ± 0.2
t-channel Contribution (%)	12.2 ± 0.3	0	0	13.1 ± 0.3
Backgrounds:				
e^+e^- (%)	–	< 0.03	1.1 ± 0.1	–
$\mu^+\mu^-$ (%)	< 0.11	–	0.12 ± 0.08	–
$\tau^+\tau^-$ (%)	1.18 ± 0.07	0.12 ± 0.08	–	–
Hadrons (%)	0	0	1.12 ± 0.31	0.8 ± 0.07
Two-photon (%)	0	0	0.66 ± 0.13	0.22 ± 0.04
Cosmic Rays (%)	0	0.23 ± 0.05	0.07 ± 0.02	0.02 ± 0.01
Total Sys. Error $\sqrt{s} = M_Z$ (%)	0.5	0.5	0.9	0.4

3.1 $Z \to \ell^+\ell^-$

The selection of leptons without distinguishing the lepton flavour is done in a manner similar to that described in [1] except that the angular acceptance of the selection is increased to $|\cos\theta^*| < 0.9$. To further reduce the background from cosmic rays and two-photon interactions, some criteria are added to the requirements described above.

Cosmic-ray background is reduced by requiring that for two track events, at least one track originate from the beam crossing within 1 cm in the transverse direction and 5 cm in the beam direction. Also, $\ell^+\ell^-$ candidates are required to have at least 4 ITC points associated to a track; this requirement rejects most cosmic-ray events because of the more restrictive timing of the ITC.

Two-photon background is suppressed by the following requirements:

- The transverse momentum relative to the beam of the vector sum of the tracks in each hemisphere (the jet transverse momentum) must be larger than 2.5 GeV in at least one hemisphere.
- For two-track events with both momenta less than 6 GeV, the transverse momenta of the two tracks with respect to the beam must differ from each other by more than 15%.
- The visible invariant mass of the event must be greater than 4.5 GeV.

Using the above criteria, 24,757 events are selected as lepton-pair candidates with an efficiency of (98.3 ± 0.2)% inside the angular range $|\cos\theta^*| < 0.9$. The remaining two-photon background of (9.9 ± 1.9) pb (corresponding to (0.22 ± 0.04)% of the selected event sample at the peak) has been subtracted.

The main systematic errors in the common-lepton cross section result from uncertainties in the angular acceptance and acollinearity cut (0.14%), the t-channel contribution (0.3%), and the track parameters, such as momentum errors (0.16%, which is included in the quoted systematic error in selection efficiency). Combining errors in quadrature, the total systematic error is less than 0.4%.

[3] In this table, the selection efficiency is defined as the efficiency within the accepted angular range.

3.2 $Z \rightarrow e^+e^-(\gamma)$

The selection of electron pairs is based on the sum of the momenta of the two most energetic tracks in an event and on the sum of energies of the ECAL clusters associated with these tracks [1]. The current analysis includes energy which escapes through cracks in the ECAL but is detected by the HCAL, and includes the energy of radiated photons. As shown in Fig. 3, much of the energy lost in ECAL cracks is recovered in the HCAL. When ECAL clusters are close to an ECAL crack, the HCAL energy which is associated to the ECAL cluster is included in the energy sum. This procedure is applied only to two-track events; the background from $\tau^+\tau^-$ pairs would be increased by about a factor two if the procedure were applied to higher multiplicity events.

The $e^+e^-(\gamma)$ candidates must satisfy the following requirements:

$$\begin{aligned} \sum E &> 0.20\sqrt{s} \\ \sum p &> 0.05\sqrt{s} \\ \sum p + \sum \mathcal{E} &> 1.2\sqrt{s}. \end{aligned}$$

Here, $\sum p$ refers to the sum of the momenta of the two most energetic tracks and $\sum E$ ($\sum \mathcal{E}$) refers to the energy sum of the clusters associated with these tracks before (after) the inclusion of energy from a radiated photon and of the associated HCAL energy.

This selection yields a sample of 6,947 events in the angular range $-0.9 < \cos\theta^* < +0.7$. The efficiency of the selection within the geometrical acceptance is calculated to be $(98.8 \pm 0.3)\%$ from Monte Carlo [7]. The dominant background in the electron sample comes from $\tau^+\tau^-$ pairs and is estimated to be $(1.18 \pm 0.07)\%$ from Monte Carlo simulation [8].

The systematic error in the selection efficiency and background has been estimated from the variation of the number of accepted events for data and Monte Carlo [7,8] as a function of the most sensitive cut, $\sum p + \sum \mathcal{E}$, and has been found to be 0.3% inside the acceptance (Fig. 4).

The other important systematic error comes from the t-channel subtraction. At the peak energy, uncertainties in ALIBABA result in a systematic error of 2% of the pure t-channel part of the subtracted cross section; the uncertainty in the value of $\sqrt{s} - M_Z$ (10 MeV) gives an additional contribution to the systematic error of 1.6% of the subtracted cross section in the angular range $-0.9 < \cos\theta^* < +0.7$. This contribution to the systematic error would be larger, i.e. 1.2% of the subtracted cross section (about 30% of the total cross section), in the range $|\cos\theta^*| < 0.9$. Away from the peak, the latter error is negligible and the total systematic error is estimated to be 2% of the pure t-channel part of the cross section. Since this relative error in the t-channel subtraction varies slowly across the Z peak, the value at the peak has been used. The 0.7% systematic error in the absolute luminosity [3] introduces a further systematic uncertainty in the t-channel subtraction.

The total systematic error in the cross section is about 60% of the statistical error at the peak and less than 20% away from the peak. The systematic uncertainty in the forward-backward asymmetry is about 10% of the statistical error.

3.3 $Z \rightarrow \mu^+\mu^-(\gamma)$

The muon-pair selection has been extended in two respects since the previous analysis [1]. The muon chambers[4] are now used in conjunction with the HCAL to identify muons, and the kinematic

[4]One double-layer of muon chambers surrounding the hadronic calorimeter has been installed for the 1990 period. The muon chambers, which are constructed of streamer tubes with a 1 cm pitch, provide a single 3-dimensional space point for charged tracks which penetrate the 7.5 interaction lengths of material between the chambers and the interaction point at normal incidence.

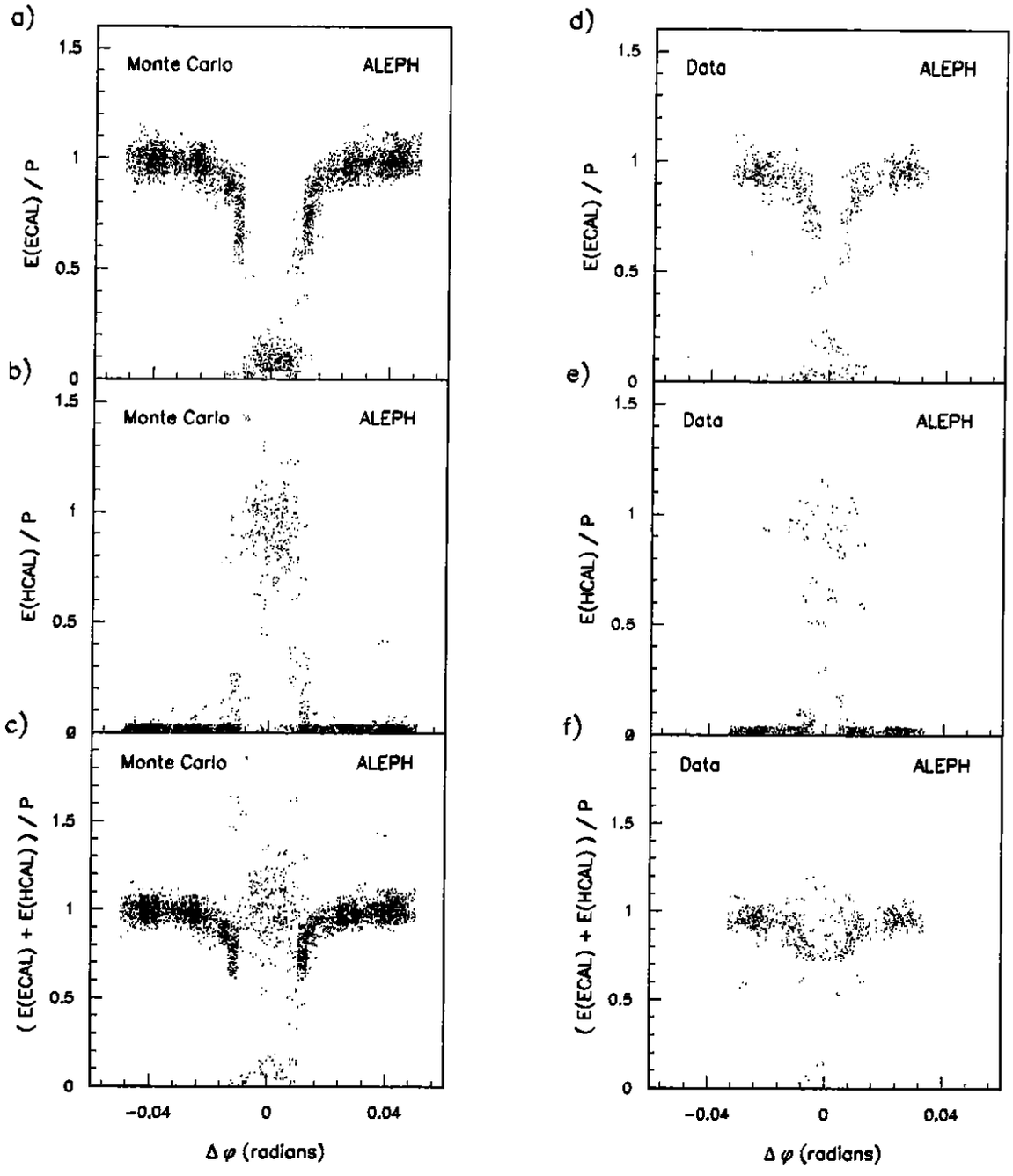

Figure 3: a) ECAL barrel energy versus azimuth $\Delta\varphi$, the distance to the crack, for Bhabha candidates, b) HCAL barrel energy versus azimuth $\Delta\varphi$ for Bhabha candidates, c) the sum of a) and b), for Monte Carlo; d), e) and f) are the equivalent plots for data. The 12 modules in φ have been plotted together and only the part of the φ range around the crack regions is shown.

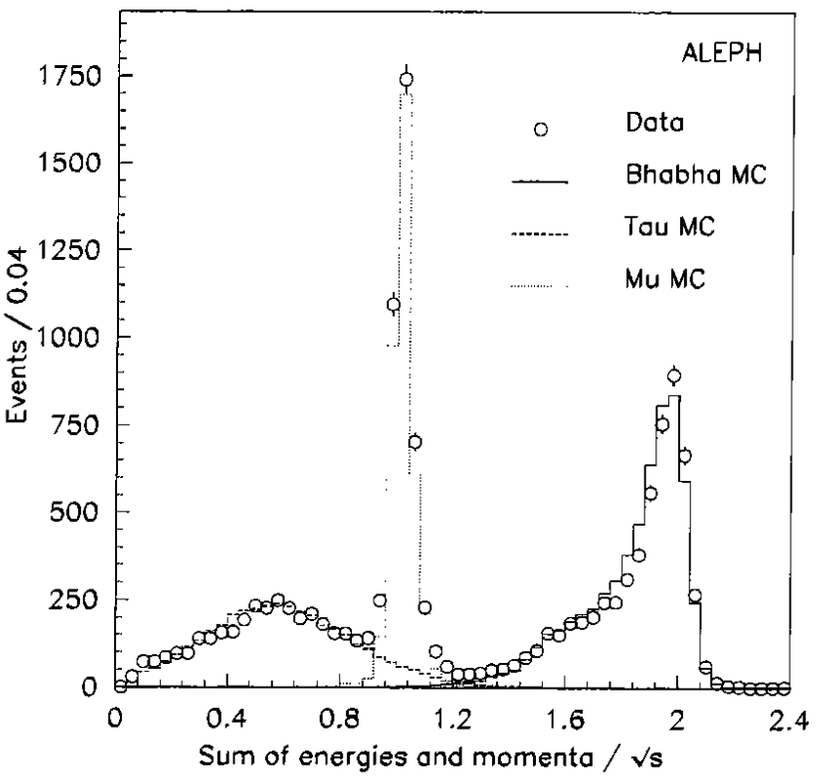

Figure 4: $\sum p + \sum \mathcal{E}$ for lepton pairs, together with Monte Carlo predictions from the different lepton species.

requirements of the selection have been changed to improve the efficiency for events with a radiated photon. If the momenta of the two fastest tracks both exceed $35\sqrt{s}/M_Z$ GeV, the event is accepted as a muon-pair candidate. If only one track exceeds this momentum cut, the event is accepted if a photon can be found which is consistent in energy and position with the $\mu^+\mu^-\gamma$ hypothesis. Figure 5 shows the photon-energy distribution for the selected events; the Monte Carlo [8] distribution is consistent with the data. In the current selection one of the two highest momentum tracks is required to have an HCAL hit pattern consistent with that expected for a muon (as described in [1]), or to be matched to a hit in the muon chambers.

A total of 6,691 $\mu^+\mu^-$ candidates has been selected in the angular range $|\cos\theta^*| < 0.9$. The efficiency of the selection in this angular range is $(98.4 \pm 0.5)\%$. The backgrounds in the sample are $\tau^+\tau^-$ pairs and cosmic-ray events. The $\tau^+\tau^-$ background has been calculated from Monte Carlo [8] to be $(0.12 \pm 0.08)\%$. The cosmic-ray background has been estimated to be (3.3 ± 0.7) pb (corresponding to $(0.23 \pm 0.05)\%$ of the selected event sample at the peak) by loosening vertex requirements and using the number of additional events found to estimate the number of background events accepted by the standard vertex requirements.

In order to estimate the systematic error of the event selection based on HCAL, the cross-sections obtained with this selection are compared with those obtained by a selection based on the presence of minimum ionizing particle signals in ECAL and HCAL. A systematic error of 0.2% is assigned to the cross sections to account for the observed difference of $(0.1 \pm 0.2)\%$.

The Monte Carlo generator used to measure the efficiency of the kinematic cuts does not include all higher-order radiative corrections, and therefore underestimates the number of events in which two hard photons are produced by final state radiation. The comparison of the number of $\mu^+\mu^-\gamma$ events found in data and in Monte Carlo shows a disagreement of about 10% on 3.5% of the

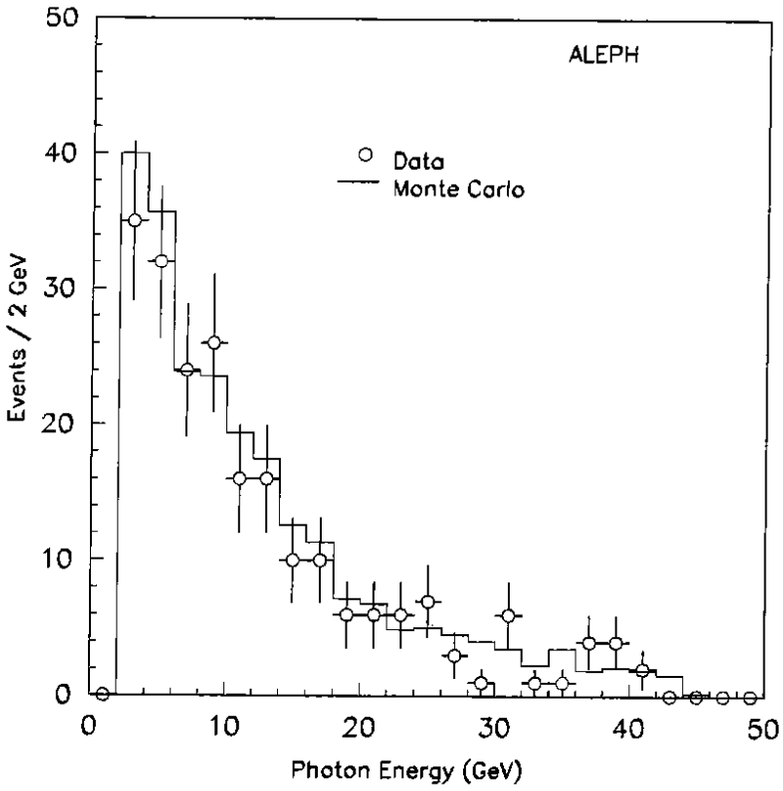

Figure 5: Photon-energy distribution for $\mu^+\mu^-\gamma$ events from data and Monte Carlo.

selected event sample; the resulting systematic uncertainty is estimated to be 0.35%. Combining this uncertainty with the statistical error in the determination of the efficiency of the kinematic cuts gives a total systematic error of 0.5% in this efficiency. To check this value, the cross sections have been compared with those obtained when relaxing the momentum cut on the second track from $35\sqrt{s}/M_Z$ GeV to $22\sqrt{s}/M_Z$ GeV. The average difference is $(0.3 \pm 0.2)\%$, which is consistent with the quoted systematic error.

Including the 0.2% uncertainty in backgrounds, a 0.6% systematic error is assigned to the $\mu^+\mu^-$ cross section, in addition to the systematic uncertainty in the luminosity measurement.

To estimate the systematic error in the forward-backward asymmetry, results obtained with two sets of kinematic cuts and two sets of selection cuts (as described above) have been compared. The average difference in the asymmetry between the two selection methods is 0.002 ± 0.004; the average difference between the two sets of kinematic cuts is 0.002 ± 0.003. The resulting systematic error in the forward-backward asymmetry is about 30% of the statistical error at the peak and less than 10% away from the peak.

3.4 $\mathbf{Z} \rightarrow \tau^+\tau^-$

The $\tau^+\tau^-$ selection procedure used for the cross-section measurement is similar to that described in Ref. [1]. The requirements are those of the common-lepton selection together with additional cuts to separate $\tau^+\tau^-$ candidates from e^+e^- and $\mu^+\mu^-$ events. In particular, the $\tau^+\tau^-$ candidates are required to satisfy the criteria described below.

To suppress e^+e^- and $\mu^+\mu^-$ events, the square of the missing mass calculated from the tracks (assuming pion masses) and $\sqrt{s}$ is required to exceed $400\sqrt{s}/M_Z$ GeV^2. The e^+e^- background is reduced further by requiring that the energy measured in ECAL be less than $55\sqrt{s}/M_Z$ GeV.

This selection yields a sample of 6,260 events with $|\cos\theta^*| < 0.9$. The efficiency of the selection within the geometrical acceptance is $(86.4\pm0.8)\%$; the inefficiency results from the missing mass and ECAL energy cuts in equal proportions. The main backgrounds are $Z \to q\bar{q}$, $Z \to e^+e^-$, and two-photon events. The $q\bar{q}$ and two-photon background has been determined from Monte Carlo [9,10]. A background of $(1.12 \pm 0.31)\%$ for $q\bar{q}$ and (9.9 ± 1.9) pb (*i.e.*, $(0.66 \pm 0.13)\%$ of the selected event sample at the peak) for two-photon events has been subtracted from the cross sections. The remaining background results mainly from e^+e^- pairs where two photons are radiated, producing a large missing mass, and at the same time part of the electromagnetic energy is lost either in inactive parts of ECAL or because the photons are collinear with the initial electrons. This background was measured by applying the $\tau^+\tau^-$ selection to the e^+e^- sample of events obtained using the described $Z \to e^+e^-(\gamma)$ selection, and taking the efficiencies of the two selections into account. The small $\tau^+\tau^-$ contamination in the e^+e^- data has been estimated by Monte Carlo. The e^+e^- background was found to be $(1.1 \pm 0.5)\%$ and has been subtracted.

The systematic error in the selection efficiency has been evaluated with data. The following procedure is used to produce an unbiased sample of $\tau^+\tau^-$ events by combining taus from different events. Only events with less than 7 charged tracks and at least one track per hemisphere are considered. The energy sum of the charged tracks is required to be larger than 8 GeV and the acollinearity less than 30°. A τ selection procedure is applied to each event hemisphere. If there is only one charged track in a hemisphere, the sum of energy of the charged track and ECAL energy must be less than 35 GeV; if there are 2 or 3 charged tracks, in addition, the invariant mass of the tracks must be less than 2 GeV. If such a τ candidate is found in an event, only the τ in the opposite hemisphere is used in the study. Half events having opposite charge and nearly opposite polar and azimuthal angles are paired to form complete events with unbiased ECAL energy and missing mass distributions. Figure 6 shows these distributions compared to those of $\tau^+\tau^-$ Monte Carlo events. The efficiency observed in the mixed-event sample confirms that determined with the $\tau^+\tau^-$ Monte Carlo within the 0.6% statistical precision of the comparison. The event-mixing method destroys the intrinsic correlation of helicities between two taus of a real event. This effect has been studied with Monte Carlo and found to be negligible.

To measure the forward-backward asymmetry, a more selective procedure has been adopted since a charge-asymmetric background can produce a bias in the measurement. To reduce the already small contamination of e^+e^- events, a selection procedure which positively identifies τ decays based on muon and pion identification is used. For each track with momentum larger than 3 GeV, the same muon identification as used in the $\mu^+\mu^-$ selection is applied. If the track cannot be identified as a muon, the charged-pion hypothesis is tested. A pion is distinguished from an electron on the basis of either its ECAL energy deposit, if its momentum is larger than 3 GeV, or its dE/dx measurement in the TPC.

In addition, reconstructed π^0s with the energy of each photon greater than 250 MeV are used; details of the π^0 identification are given in reference [11]. An event is accepted as a $\tau^+\tau^-$ candidate if either at least one muon, or at least two pions (including π^0s), or one pion with an ECAL energy ($E_{\rm ECAL}$) less than $0.8E_{\rm beam}$ in each hemisphere of the event are identified. 6,095 $\tau^+\tau^-$ candidates are selected with an efficiency of 80.8% inside the defined acceptance. The remaining e^+e^- background is $(0.23\pm0.12)\%$; it has been measured directly from data by tagging an electron (or positron) in one hemisphere of the event and counting the number of identified pions in the other hemisphere. Figure 7 shows the probability of identifying either one muon or one or more pions in one hemisphere once an electron has been tagged in the other hemisphere; the same probability for an unbiased sample of $\tau^+\tau^-$ Monte Carlo events is shown also.

For the measurement of $A_{\rm FB}$ in the $\tau^+\tau^-$ channel, the $\mu^+\mu^-$ and $q\bar{q}$ background can be neglected while the small e^+e^- background has been subtracted. The systematic error in the forward-

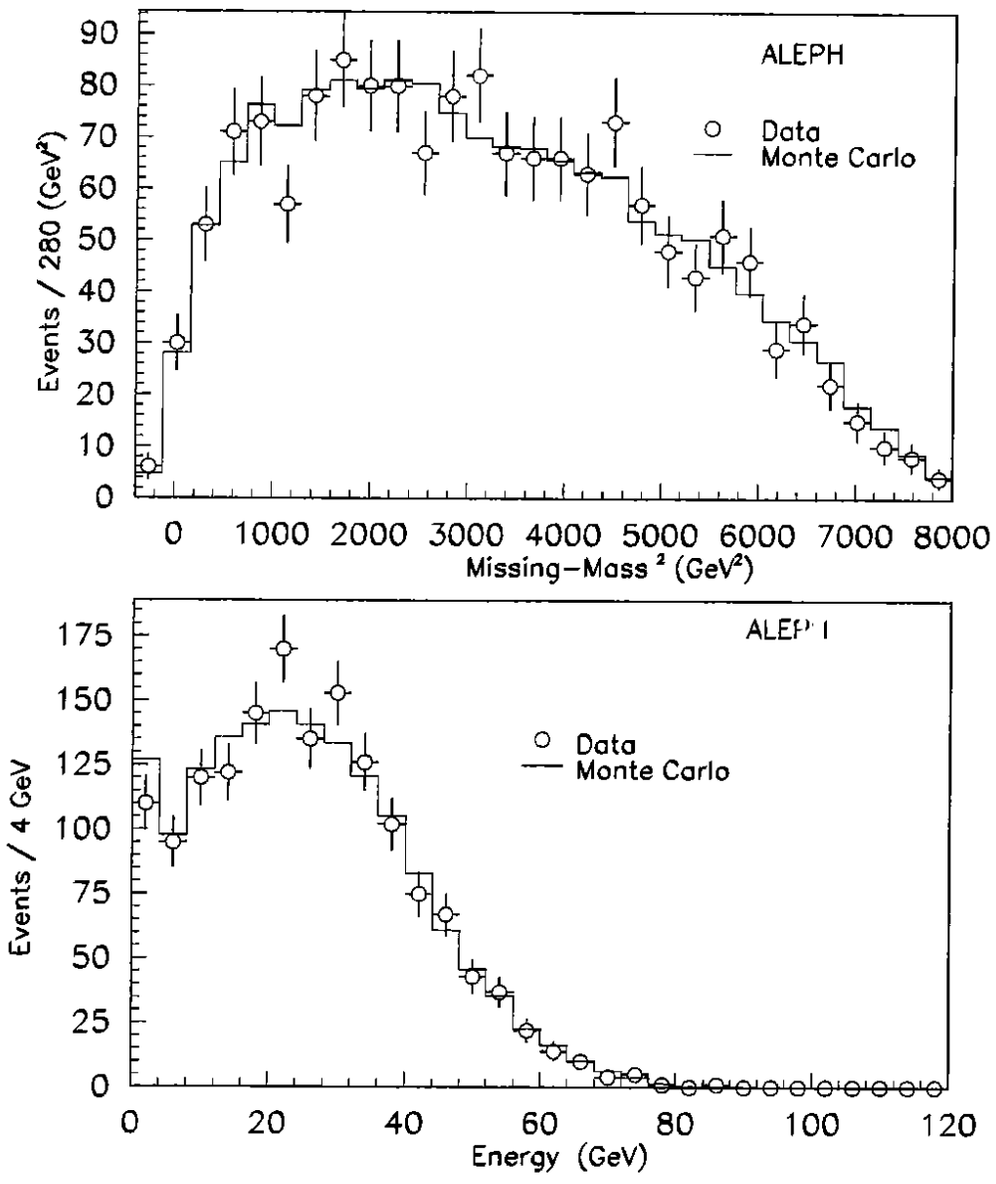

Figure 6: a) Missing-mass squared distribution for $\tau^+\tau^-$ Monte Carlo (histogram) and paired half events from data (solid circles); b) ECAL energy distribution for $\tau^+\tau^-$ Monte Carlo and paired half events from data.

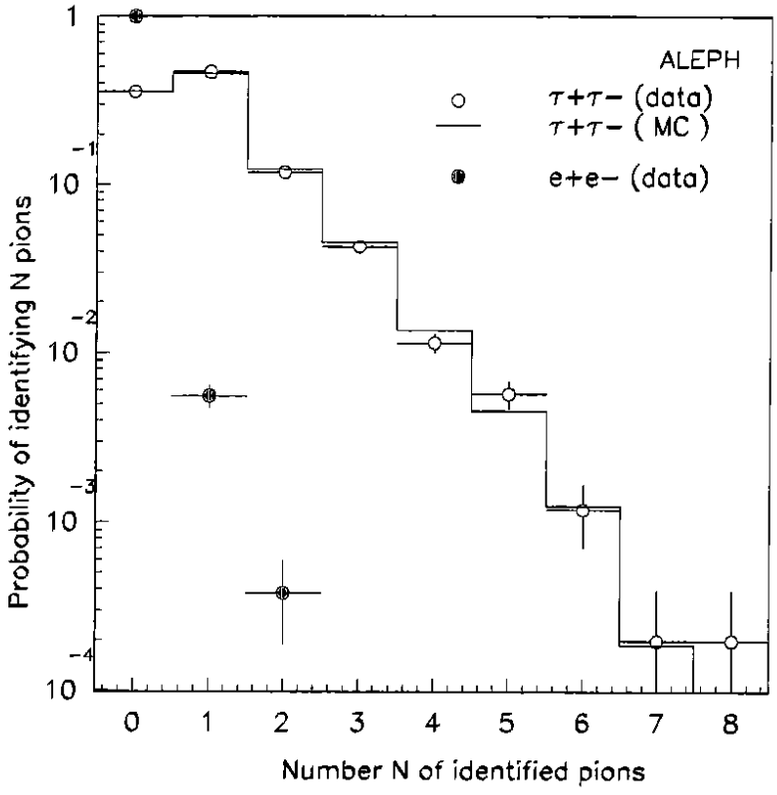

Figure 7: Probability of identifying N pions in one hemisphere for the $\tau^+\tau^-$ sample (open circles) and for the e^+e^- sample (solid circles). The Monte Carlo $\tau^+\tau^-$ sample is shown as a solid histogram.

backward asymmetry, resulting mainly from uncertainty in the e^+e^- background subtraction, is about 2% of the statistical error at all centre-of-mass energies.

4 Comparison among Lepton Channels

As discussed earlier, a substantial background in the separate lepton analyses comes from other lepton channels. To check the estimated efficiency and background for each lepton channel, the selections are compared among themselves and with the common-lepton selection. Figure 8 shows the number of events in the regions of overlap among the different selections.

Only data from the 1990 running period and with $|\cos\theta^*| < 0.9$ are used for this comparison. 18 events out of 22,031 events found in either the individual or the common-lepton selections do not appear in the common-lepton sample. These 18 events consist of 5 e^+e^- and 13 $\mu^+\mu^-$ candidates. In this comparison, one must consider the different methods of cosmic-ray rejection used by the $Z \to \mu^+\mu^-$ and $Z \to \ell^+\ell^-$ analyses. The 7 events rejected by the ITC hit requirement in the common-lepton selection are consistent with the higher cosmic-ray background in the $Z \to \mu^+\mu^-$ selection. Subtracting these 7 events leaves a discrepancy of 11 events out of 22,031, *i.e.*, 0.05%.

A total of 803 events are found in the common-lepton sample but not in the separate lepton samples. The events are consistent with being leptonic Z decays and represent less than 4% of the events found by the individual selections. Although these events are difficult to identify individually, one can estimate the expected contribution of each lepton species by taking into account the relative efficiencies of selecting e^+e^-, $\mu^+\mu^-$ or $\tau^+\tau^-$ inside the common-lepton sample and the relevant

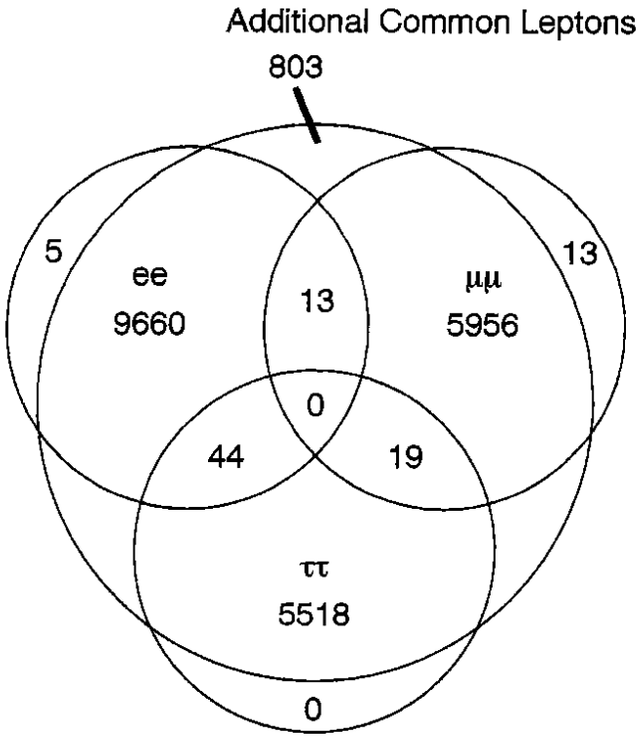

Figure 8: Comparison of leptonic event selections for 1990 period.

backgrounds. The total expected contribution is 760 ± 23 events (110 ± 10 e^+e^-, 82 ± 16 $\mu^+\mu^-$, 568 ± 13 $\tau^+\tau^-$), and is statistically consistent with the 803 events observed. Thus, the separate and common-lepton selections agree at the level of $(0.2 \pm 0.1)\%$.

Events which are present in more than one lepton selection have been studied also. There are no events which pass the selection requirements for all three lepton species, and there are no events passing two selections which are not also present in the common-lepton sample.

Taking into account the estimated background in each sample and the "conditional" efficiencies of selecting events as candidates of one type when they have already been selected as candidates of another type, the number of events expected to be common to different pairs of selections can be calculated. For the e^+e^- and $\tau^+\tau^-$ species, where the overlap between the two species is large, the "conditional" efficiencies have been obtained from Monte Carlo [7,8]. For all other "conditional" efficiencies, it has been assumed that these efficiencies were equivalent to the background of one species inside the other (see Table 2). A total of 50 ± 6 events are expected to be common to the e^+e^- and $\tau^+\tau^-$ samples, statistically consistent with the 44 events found. Less than 9 events are expected to be common to e^+e^- and $\mu^+\mu^-$ selections and 13 events have been found. Less than 17 events are expected to be common to the $\mu^+\mu^-$ and $\tau^+\tau^-$ selections and 19 events have been found. All the events appearing in more than one individual lepton selection have been scanned visually, and the observed numbers of events in each category are consistent with these estimates. The largest discrepancy between the measured and predicted numbers of events in any overlap region is 0.1%.

Table 3: Hadron and Lepton Cross Sections. Only statistical errors are given.

$\sqrt{s}$ (GeV)	$\mathcal{L}_{\rm int}$ ($\rm nb^{-1}$)	$\sigma_{\rm had}$ (nb)	σ_{ee} (nb)	$\sigma_{\mu\mu}$ (nb)	$\sigma_{\tau\tau}$ (nb)	$\sigma_{\ell\ell}$ (nb)
88.224	482.2 ± 4.1	4.596 ± 0.105	0.233 ± 0.039	0.247 ± 0.025	0.171 ± 0.024	0.599 ± 0.063
88.277	108.5 ± 2.0	4.534 ± 0.220	0.324 ± 0.088	0.228 ± 0.050	0.352 ± 0.072	1.027 ± 0.152
89.220	520.3 ± 4.3	8.409 ± 0.146	0.334 ± 0.042	0.502 ± 0.034	0.387 ± 0.034	1.279 ± 0.074
89.277	46.5 ± 1.3	8.865 ± 0.503	0.439 ± 0.150	0.288 ± 0.089	0.480 ± 0.127	1.260 ± 0.246
90.222	447.1 ± 4.1	18.464 ± 0.265	0.924 ± 0.063	0.902 ± 0.050	0.882 ± 0.054	2.751 ± 0.104
90.277	72.6 ± 1.6	19.823 ± 0.691	1.135 ± 0.170	0.953 ± 0.109	0.790 ± 0.127	2.811 ± 0.260
91.030	144.3 ± 2.3	29.254 ± 0.657	1.527 ± 0.133	1.312 ± 0.099	1.384 ± 0.118	4.262 ± 0.217
91.222	3655.7 ± 11.8	30.502 ± 0.135	1.489 ± 0.026	1.432 ± 0.022	1.494 ± 0.024	4.432 ± 0.044
91.277	137.6 ± 2.3	30.357 ± 0.692	1.249 ± 0.123	1.412 ± 0.109	1.319 ± 0.117	4.151 ± 0.218
91.529	142.8 ± 2.5	30.918 ± 0.691	1.539 ± 0.131	1.510 ± 0.109	1.406 ± 0.119	4.419 ± 0.217
92.216	555.6 ± 4.7	21.762 ± 0.271	1.093 ± 0.055	1.003 ± 0.047	1.060 ± 0.053	3.146 ± 0.091
92.277	112.4 ± 2.1	21.346 ± 0.594	1.055 ± 0.119	1.072 ± 0.109	1.075 ± 0.118	3.259 ± 0.207
93.220	597.5 ± 4.9	12.410 ± 0.177	0.634 ± 0.040	0.634 ± 0.036	0.552 ± 0.037	1.861 ± 0.069
93.277	42.7 ± 1.3	12.623 ± 0.670	0.760 ± 0.164	0.685 ± 0.139	0.514 ± 0.138	2.175 ± 0.276
94.215	641.7 ± 5.1	7.989 ± 0.128	0.406 ± 0.032	0.437 ± 0.029	0.409 ± 0.031	1.230 ± 0.056
94.278	66.9 ± 1.6	7.989 ± 0.399	0.452 ± 0.104	0.347 ± 0.079	0.389 ± 0.096	1.025 ± 0.161

5 Cross Sections and Forward-backward Asymmetries

Data have been collected at 16 energies at and near the peak of the Z resonance. Table 3 summarizes the cross sections for hadrons and lepton pairs as a function of centre-of-mass energy; the seven highest luminosity points correspond to data taken during 1990. Only statistical errors are given; the systematic errors resulting from the event selection requirements are summarized in Tables 1 and 2. The cross sections given in Table 3 have been corrected for the effect of the center-of-mass energy spread of LEP, as described in the following section.

The luminosity, which is measured with small-angle Bhabhas [3], has an experimental error of 0.6%. The theoretical calculation for small angle Bhabha scattering includes corrections of second order in α [12,13]. The uncertainty in this calculation within the acceptance is 0.3% [3], giving a total luminosity error of 0.7%.

Table 4 summarizes the forward-backward asymmetries for lepton pairs as a function of centre-of-mass energy. The systematic errors are negligible compared to the statistical errors. The determination of the cross section and of the forward-backward asymmetry from the angular distribution is not strictly model independent because of the subtraction of the t-channel contribution; this effect, however, is negligible with respect to the quoted systematic error. The systematic uncertainty in the measurement of the forward-backward asymmetry resulting from the LEP beam-energy uncertainty [14] is negligible compared to the statistical error.

6 Z Resonance Parameters

The cross section $\sigma_{e^+e^-\to f\bar{f}}$ for fermion-pair production in e^+e^- annihilation, after correction for initial-state radiation, can be expressed in a model-independent formulation [15,16,17,18] as a function of the physical parameters of the Z resonance. It contains three terms: the Z-exchange contribution which is represented by a Breit-Wigner function, the photon-exchange contribution,

Table 4: Forward-backward asymmetries as a function of the centre-of-mass energy for $Z \rightarrow$ lepton pairs.

$\sqrt{s}(GeV)$	$A_{\rm FB}^{e^+e^-}$	$A_{\rm FB}^{\mu^+\mu^-}$	$A_{\rm FB}^{\tau^+\tau^-}$	$A_{\rm FB}^{\ell^+\ell^-}$
88.224	-0.389 ± 0.228	-0.132 ± 0.103	-0.268 ± 0.123	-0.319 ± 0.098
88.277	-0.195 ± 0.357	-0.341 ± 0.196	-0.582 ± 0.140	-0.356 ± 0.167
89.220	-0.512 ± 0.187	-0.296 ± 0.062	-0.129 ± 0.082	-0.259 ± 0.060
89.277	-1.168 ± 0.856	-0.304 ± 0.203	-0.330 ± 0.200	-0.903 ± 0.281
90.222	-0.170 ± 0.082	-0.159 ± 0.052	-0.084 ± 0.062	-0.123 ± 0.037
90.277	-0.123 ± 0.172	-0.142 ± 0.129	-0.020 ± 0.130	-0.147 ± 0.093
91.030	$+0.065 \pm 0.090$	$+0.016 \pm 0.074$	-0.049 ± 0.082	$+0.027 \pm 0.049$
91.222	-0.009 ± 0.018	-0.002 ± 0.015	$+0.021 \pm 0.016$	-0.002 ± 0.009
91.277	-0.035 ± 0.110	-0.058 ± 0.076	$+0.019 \pm 0.084$	-0.040 ± 0.050
91.529	-0.102 ± 0.092	-0.011 ± 0.076	$+0.018 \pm 0.079$	-0.029 ± 0.047
92.216	$+0.145 \pm 0.049$	$+0.108 \pm 0.046$	$+0.130 \pm 0.050$	$+0.130 \pm 0.027$
92.277	$+0.030 \pm 0.120$	$+0.106 \pm 0.091$	$+0.184 \pm 0.101$	$+0.085 \pm 0.061$
93.220	$+0.237 \pm 0.058$	$+0.149 \pm 0.054$	$+0.270 \pm 0.059$	$+0.197 \pm 0.035$
93.277	$+0.200 \pm 0.218$	$+0.287 \pm 0.179$	$+0.415 \pm 0.192$	$+0.320 \pm 0.114$
94.215	$+0.130 \pm 0.078$	$+0.180 \pm 0.065$	$+0.326 \pm 0.072$	$+0.165 \pm 0.041$
94.278	$+0.242 \pm 0.250$	$+0.101 \pm 0.204$	-0.232 ± 0.220	-0.045 ± 0.147

and the interference term. In a completely model-independent description, the precise value of the interference term is unknown. The dependence of the results on this term is less than 0.1% [19], so the Standard Model value has been assumed. The effect of initial state radiation is large, of the order of 30% at the peak, but is known to better than 0.2% [16] of the cross section, and is taken into account. The peak cross section from Z exchange, when unfolded from initial-state radiation, is

$$\sigma_{ff}^0 = \frac{12\pi}{M_{\rm Z}^2} \frac{\Gamma_{ee}\Gamma_{ff}}{\Gamma_{\rm Z}^2}.$$

The resonance parameters have been determined by fitting the model-independent lineshape as implemented in the computer program MIZA [19] to the cross sections presented in Table 3. In the χ^2 minimization, the various correlations in the data which result from the common luminosity determination and common event selection criteria are taken into account. For the electron-pair sample and the common-lepton sample, points with $|\sqrt{s} - M_{\rm Z}| > 1.5$ GeV are omitted to minimize the contribution of the interference term since it depends on Γ_{ee}, and to minimize the uncertainty resulting from the t-channel subtraction.

Fitting the hadronic and three lepton-pair cross sections simultaneously, one can determine six parameters: the Z mass, $M_{\rm Z}$, the total width, $\Gamma_{\rm Z}$, the peak hadronic cross section, $\sigma_{\rm had}^0$, and the three ratios of hadron to lepton partial widths, $\Gamma_{\rm had}/\Gamma_{ee}$, $\Gamma_{\rm had}/\Gamma_{\mu\mu}$, and $\Gamma_{\rm had}/\Gamma_{\tau\tau}$. A more precise determination of $R = \Gamma_{\rm had}/\Gamma_{\ell\ell}$ is obtained from a four-parameter fit, assuming lepton universality. The results are summarized in Table 5. Additional errors resulting from uncertainty in the absolute scale of the LEP energy, the beam energy spread, non-reproducibility of energy from fill to fill, and systematic point-to-point energy uncertainties among the scan points are not shown in Table 5. The absolute scale of the centre-of-mass energy is estimated to be $2.2 \times 10^{-4}(\pm 20$ MeV) [14], which is the main uncertainty in the Z mass. The beam energy spread distorts the Z line shape. This effect has been included by convoluting the line shape with a Gaussian centre-of-mass energy spread with $\sigma = 50$ MeV at the Z peak [14]. The energy spread increases the measured total

Table 5: Fit results for hadron and lepton cross sections. Errors resulting from uncertainty in the LEP energy scale are not included.

Parameter	No lepton univ.	lepton univ.	Common-leptons	S.M. Pred. [20]
M_Z [GeV]	91.182 ± 0.009	91.182 ± 0.009	91.182 ± 0.010	
Γ_Z [GeV]	2485 ± 17	2484 ± 17	2482 ± 18	2489 ± 23
σ^0_{had}[nb]	41.44 ± 0.36	41.44 ± 0.36	41.45 ± 0.36	41.42 ± 0.07
Γ_{had}/Γ_{ee}	20.66 ± 0.33	-		
$\Gamma_{had}/\Gamma_{\mu\mu}$	21.26 ± 0.29	-		
$\Gamma_{had}/\Gamma_{\tau\tau}$	21.00 ± 0.36	-		
$\Gamma_{had}/\Gamma_{\ell\ell}$	-	21.00 ± 0.20	20.91 ± 0.20	20.80 ± 0.08
$\Gamma_{inv}/\Gamma_{\ell\ell}$	-	5.91 ± 0.15	5.93 ± 0.15	5.91 ± 0.01
χ^2	47.2 / 51 d.o.f.	49.1 / 53 d.o.f.	11.1 / 21 d.o.f.	

Table 6: Correlation coefficients for 4 parameter fit to the Z line shape assuming lepton universality.

	M_Z	Γ_Z	σ^0_{had}	R
M_Z	1	+0.06	+0.01	0.00
Γ_Z	+0.06	1	−0.31	−0.01
σ^0_{had}	+0.01	−0.31	1	+0.13
$\Gamma_{had}/\Gamma_{\ell\ell}$	0.00	−0.01	+0.13	1

width by 4 MeV and decreases the peak cross section by 0.13%. The cross sections in Table 3 are corrected for this effect. The uncertainty in the reproducibility of machine conditions from fill to fill is estimated to be 10 MeV [14]. With 7 successive 7-point scans in 1990, however, this effect contributes a negligible uncertainty of the order of 2 MeV in both the Z mass and total width. Finally, the systematic point-to-point relative energy uncertainty of 10 MeV [14] contributes an additional systematic uncertainty of 5 MeV in both the Z mass and total width.

The parameters given in Table 5 are largely independent of each other; the largest correlation is −31% between σ^0_{had} and Γ_Z, as shown in Table 6.

The four-parameter fit has been repeated with the cross sections from the common-lepton sample. The results are consistent with those found using the separate lepton samples (see Table 5) if one takes into account the angular acceptance of the common-lepton selection, which yields 20% more events.

Other parameters, including the partial widths and branching ratios, can be derived from these results (Table 7). The errors in these parameters, however, have large correlation coefficients; in particular, Γ_{ee} is strongly anticorrelated with $\Gamma_{\mu\mu}$ and $\Gamma_{\tau\tau}$. The three leptonic widths agree with each other as expected from lepton universality.

7 The Determination of Vector and Axial-vector Couplings

The leptonic width, $\Gamma_{\ell\ell}$, and the lepton forward-backward asymmetry depend on the leptonic vector and axial-vector coupling constants. In the Born approximation, the QED-corrected partial width is given by

$$\Gamma_{\ell\ell} = \frac{G_F M_Z^3}{6\sqrt{2}\pi}(g_{V\ell}^2 + g_{A\ell}^2)(1 + \frac{3}{4}\frac{\alpha}{\pi}). \qquad (3)$$

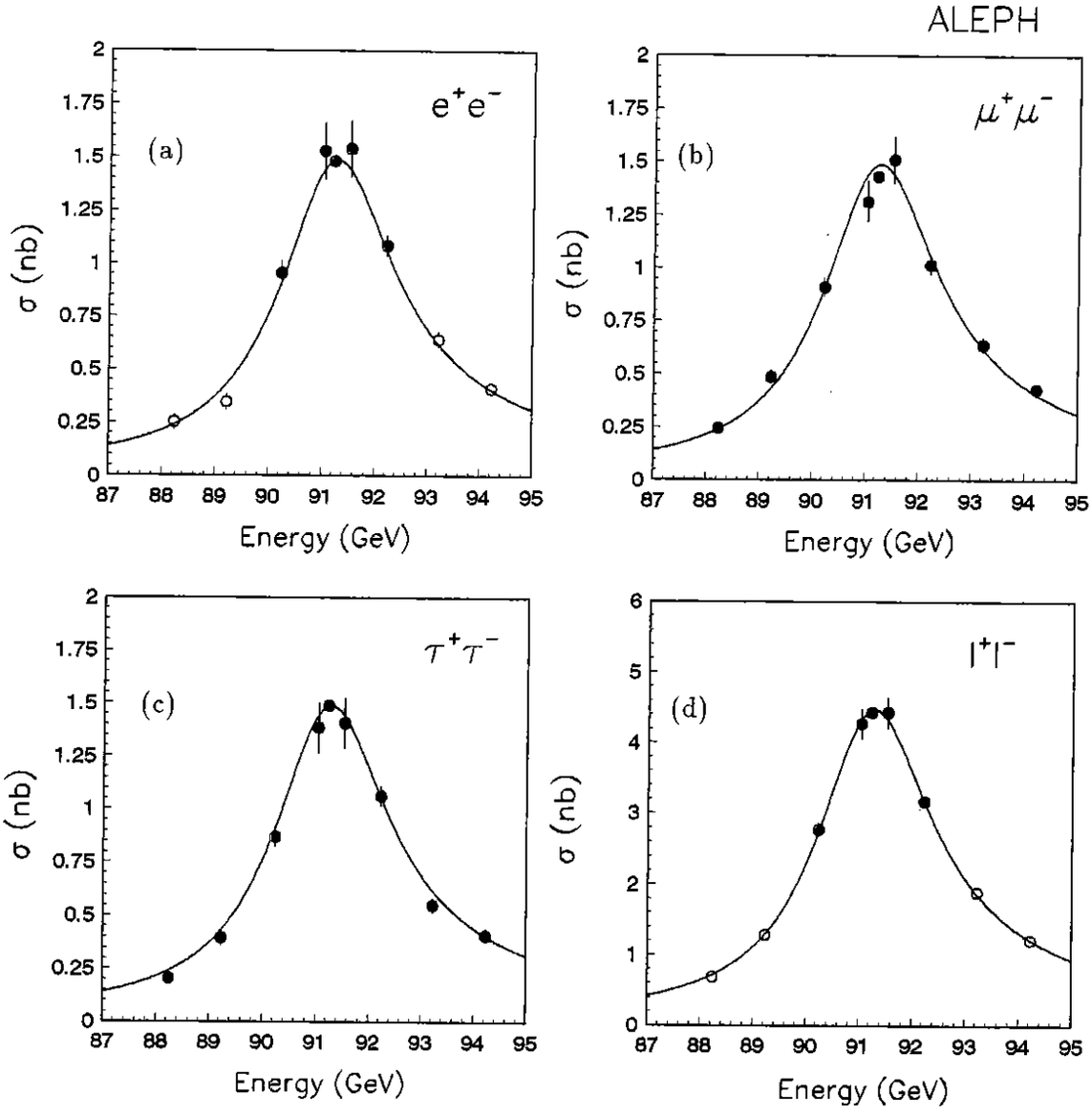

Figure 9: Cross sections for $e^+e^- \rightarrow$ lepton pairs as a function of the centre-of-mass energy: a) $e^+e^- \rightarrow e^+e^-$, b) $e^+e^- \rightarrow \mu^+\mu^-$, c) $e^+e^- \rightarrow \tau^+\tau^-$, and d) $e^+e^- \rightarrow \ell^+\ell^-$. For points where the energy difference is less than 100 MeV the average cross section is plotted. The lines are the Standard Model predictions. Points with open circles are not used in the fit.

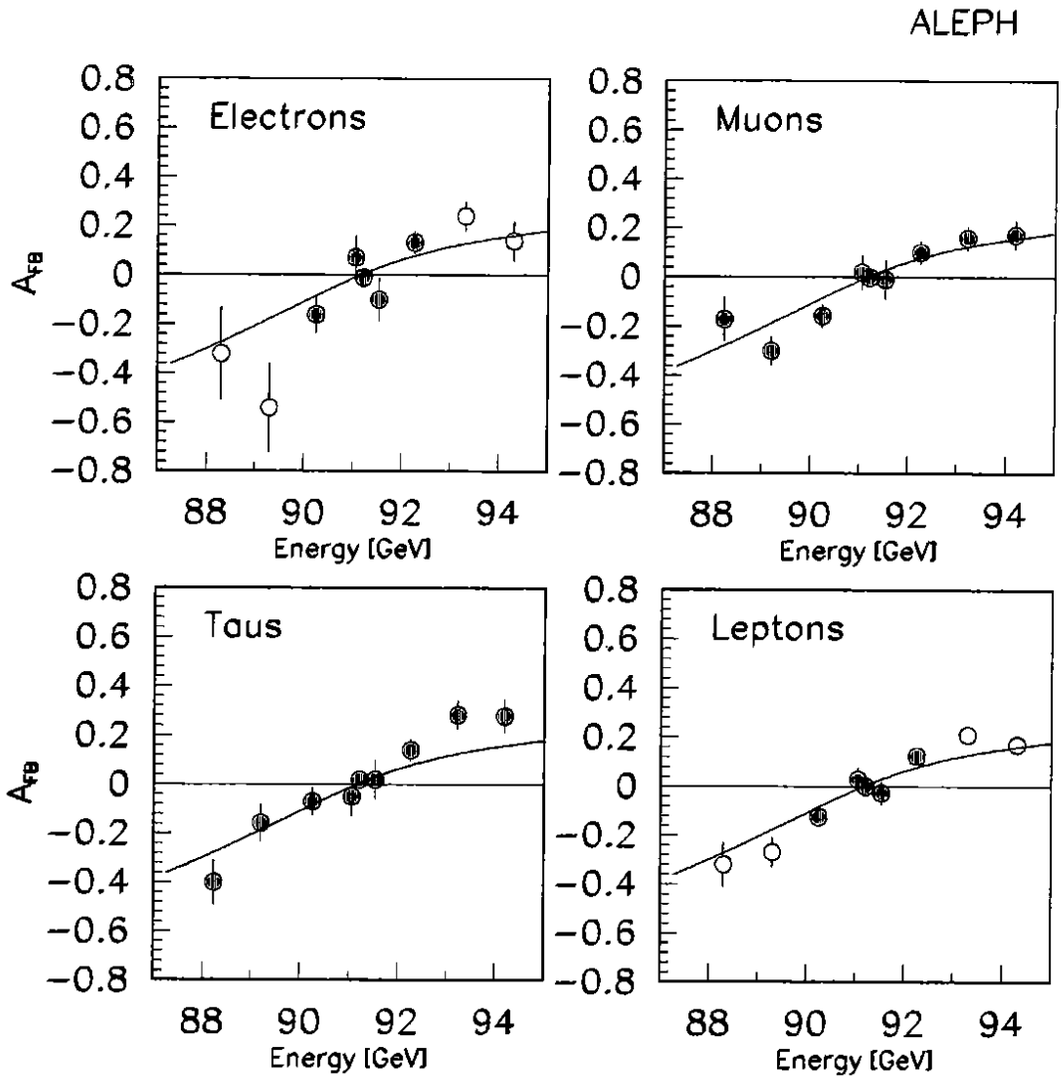

Figure 10: Forward-backward asymmetry for e^-, μ^-, τ^-, and l^- in lepton-pair events as a function of the centre-of-mass energy. For points where the energy difference is less than 100 MeV, the average asymmetry is plotted. The lines are the results of the fit. Points with open circles are not used in the fit.

Table 7: Z resonance parameters derived from the measured hadron and lepton cross sections.

Final state	Partial width (MeV)	Branching ratio	Peak cross section (nb)
	six parameter fit		
Hadrons	1730 ± 18	0.696 ± 0.006	41.44 ± 0.36
e^+e^-	83.8 ± 0.9	0.0337 ± 0.0003	2.006 ± 0.035
$\mu^+\mu^-$	81.4 ± 1.4	0.0328 ± 0.0005	1.949 ± 0.030
$\tau^+\tau^-$	82.4 ± 1.6	0.0332 ± 0.0006	1.974 ± 0.037
Invisible	507 ± 18	-	-
	four parameter fit		
Hadrons	1744 ± 15	0.702 ± 0.005	41.44 ± 0.36
Lepton	83.1 ± 0.7	0.0334 ± 0.0002	1.974 ± 0.023
Invisible	491 ± 13	-	-

The corresponding forward-backward asymmetry at the Z peak is

$$A_{\rm FB} = \frac{3}{4} \frac{2g_{\rm Ve}g_{\rm Ae}}{g_{\rm Ve}^2 + g_{\rm Ae}^2} \frac{2g_{\rm Vf}g_{\rm Af}}{g_{\rm Vf}^2 + g_{\rm Af}^2} \sim 3\frac{g_{\rm V\ell}^2}{g_{\rm A\ell}^2}. \tag{4}$$

The variation of $A_{\rm FB}$ away from the Z peak depends mainly on $g_{\rm Ae}g_{\rm Af}$.

The statistical precision of the data requires that higher-order electroweak corrections be included. In the Improved Born Approximation [21,22,23], which includes the bulk of the $O(\alpha)$ electroweak corrections, the above expressions are still valid, but the coupling constants become effective running coupling constants evaluated at $q^2 = M_{\rm Z}^2$: $g_{\rm V}(M_{\rm Z}^2)$ and $g_{\rm A}(M_{\rm Z}^2)$. These effective constants are determined from the measured partial width and asymmetry; in the limit of the Improved Born Approximation, this determination is therefore independent of the Higgs and top masses.

The measured asymmetries are fit as a function of $\sqrt{s}$, assuming lepton universality and using the lineshape measurements of $M_{\rm Z}$, $\Gamma_{\rm Z}$, and $\Gamma_{\ell\ell}$ as constraints (see the Appendix for a detailed description of the fitting formulae). In the e^+e^- channel, only the five points closest to the Z peak have been used to minimize the uncertainty resulting from t-channel subtraction.

The measured forward-backward asymmetries and the results of the fit are shown in Fig. 10. The corresponding coupling constants for leptons are

$$g_{\rm V}^2(M_{\rm Z}^2)/g_{\rm A}^2(M_{\rm Z}^2) = 0.0072 \pm 0.0027,$$

$$g_{\rm V}(M_{\rm Z}^2) = -0.042^{+0.009}_{-0.007}, \quad \text{and} \quad g_{\rm A}(M_{\rm Z}^2) = -0.498 \pm 0.002.$$

Since the leptonic width and asymmetry depend on $g_{\rm V}^2(M_{\rm Z}^2)$ and $g_{\rm A}^2(M_{\rm Z}^2)$, the signs of $g_{\rm V}(M_{\rm Z}^2)$ and $g_{\rm A}(M_{\rm Z}^2)$ have been inferred from other ALEPH measurements [11,24], and from neutrino-electron scattering experiments [25,26,27,28].

The fit can be repeated without assuming lepton universality, by replacing the constraint from $\Gamma_{\ell\ell}$ by Γ_{ee}, $\Gamma_{\mu\mu}$, and $\Gamma_{\tau\tau}$. In addition, the measurement of the τ polarization [11] is used to constrain the τ coupling further. The coupling constants as given in Table 8 are consistent with lepton universality. The smaller error in $g_{\rm V}(M_{\rm Z}^2)$ for the τ is a result of the inclusion of the τ polarization measurement. The probability contours for $g_{\rm A}(M_{\rm Z}^2)$ and $g_{\rm V}(M_{\rm Z}^2)$ are shown in Fig. 11.

Table 8: Effective vector- and axial-vector coupling constants for e, μ, and τ from forward-backward asymmetries without/with τ polarization [11].

	$A_{\rm FB}$ only		$A_{\rm FB} + P_\tau$	
	$g_{\rm V}(M_{\rm Z}^2)$	$g_{\rm A}(M_{\rm Z}^2)$	$g_{\rm V}(M_{\rm Z}^2)$	$g_{\rm A}(M_{\rm Z}^2)$
e	$-0.035^{+0.013}_{-0.014}$	$-0.501^{+0.003}_{-0.003}$	$-0.045^{+0.013}_{-0.011}$	$-0.500^{+0.003}_{-0.003}$
μ	$-0.023^{+0.029}_{-0.037}$	$-0.494^{+0.005}_{-0.004}$	$-0.018^{+0.023}_{-0.026}$	$-0.494^{+0.004}_{-0.004}$
τ	$-0.104^{+0.040}_{-0.066}$	$-0.486^{+0.019}_{-0.009}$	$-0.045^{+0.010}_{-0.011}$	$-0.495^{+0.005}_{-0.005}$
Lepton	$-0.042^{+0.009}_{-0.007}$	$-0.498^{+0.002}_{-0.002}$	$-0.041^{+0.007}_{-0.006}$	$-0.498^{+0.002}_{-0.002}$

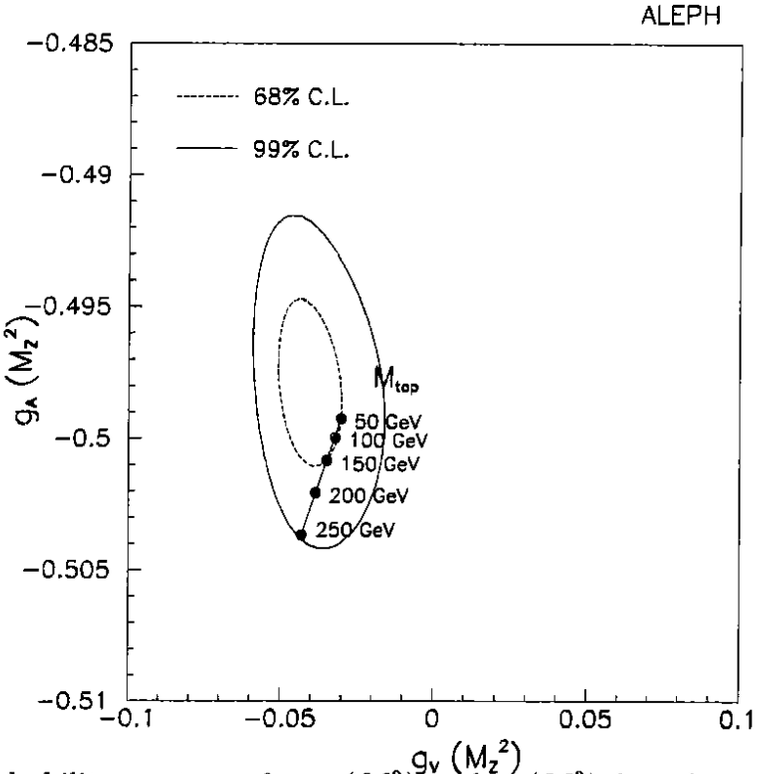

Figure 11: Probability contours for $g_{\rm V}(M_{\rm Z}^2)$ and $g_{\rm A}(M_{\rm Z}^2)$ from leptonic forward-backward asymmetries and τ polarization. The points are the expectations of the Standard Model for different top masses, assuming $\alpha_s = 0.12$ and $M_{\rm Higgs} = 200$ GeV.

8 Standard-Model Interpretation

8.1 The Number of Light Neutrino Species

The number of light neutrino species can be obtained from the measured value of $\Gamma_{\rm inv}/\Gamma_{\ell\ell}$, under the assumption that $\Gamma_{\rm inv} = N_\nu \Gamma_\nu$. In the Standard Model, $\Gamma_{\ell\ell}/\Gamma_\nu$ is related to the lepton coupling constants by

$$\frac{\Gamma_{\ell\ell}}{\Gamma_\nu} = \frac{1}{2}(1 + (\frac{g_{\rm V}(M_{\rm Z}^2)}{g_{\rm A}(M_{\rm Z}^2)})^2)(1 + \frac{3}{4}\frac{\alpha}{\pi})(1 + \delta_V), \tag{5}$$

and is equal to 0.5023 ± 0.0010 using the measured value of $g_{V\ell}/g_{A\ell}$ given in Section 7.[5] $\delta_V = -0.003 \pm 0.0003$ is the electroweak vertex correction.[6] From the present measurement

$$\Gamma_{\rm inv}/\Gamma_{\ell\ell} = \sqrt{\frac{12\pi R}{M_{\rm Z}^2 \sigma^0_{\rm had}}} - R - 3 = 5.91 \pm 0.15,$$

and the above value of $\Gamma_{\ell\ell}/\Gamma_\nu$,

$$N_\nu = 2.97 \pm 0.07.$$

The only Standard Model assumption required to obtain this result is the expression for $\Gamma_{\ell\ell}/\Gamma_\nu$; therefore, it is still valid if unexpected states yielding hadrons are present in Z decay. The expected line shapes for hadronic Z decay for 2,3, and 4 neutrino species are shown with the measured cross sections in Fig. 12.

Fixing $N_\nu = 3$, the neutrino partial width can be determined:

$$\Gamma_\nu = (163.7 \pm 4.3)\ \text{MeV}.$$

8.2 Peak Cross Sections, Ratios of Partial Widths, and α_s

The measurement of the Z mass, together with α and G_F, constrains Standard Model predictions, leaving only a small dependence on the unknown Higgs and top masses, which enter through higher-order corrections. The ratio of partial widths such as R=$\Gamma_{\rm had}/\Gamma_{\ell\ell}$ as well as the cross sections at the peak depend only weakly on $M_{\rm top}$ and $M_{\rm Higgs}$, and are therefore particularly suitable for a comparison between experiment and theory. The partial widths themselves, however, are sensitive to $\sin^2\theta_{\rm W}(M_{\rm Z}^2)$ and therefore to the top and Higgs masses.

In Fig. 13, the correlation between the peak cross section for Z decay into hadrons and R is compared with the Standard Model prediction for 2, 3, and 4 neutrino species; the agreement for $N_\nu = 3$ is good. The main uncertainty in the prediction is the uncertainty in the strong coupling constant α_s [30]. Each of the two measurements checks the Standard Model with a precision of $\sim 1\%$.

In Fig. 14, the results for $\Gamma_{\rm Z}$ and R are compared with the Standard Model. The variation of the theoretical prediction with $M_{\rm top}$ and the uncertainty resulting from the α_s correction are indicated. The agreement is good for top masses in the range 50 - 200 GeV.

The dependence of R on α_s, assuming a second-order expansion in α_s in the $\overline{\rm MS}$ scheme, is [31]

$$R = R^0(1 + \frac{\alpha_s}{\pi} + 1.41(\frac{\alpha_s}{\pi})^2),$$

[5] The Standard Model prediction [20] for $\Gamma_{\ell\ell}/\Gamma_\nu$ is 0.5022 ± 0.0008.

[6] δ_V has been obtained from [22] and [29]; the uncertainty in its value has been obtained by varying $M_{\rm top}$ from 80 GeV to 250 GeV, and $M_{\rm Higgs}$ from 50 GeV to 1 TeV.

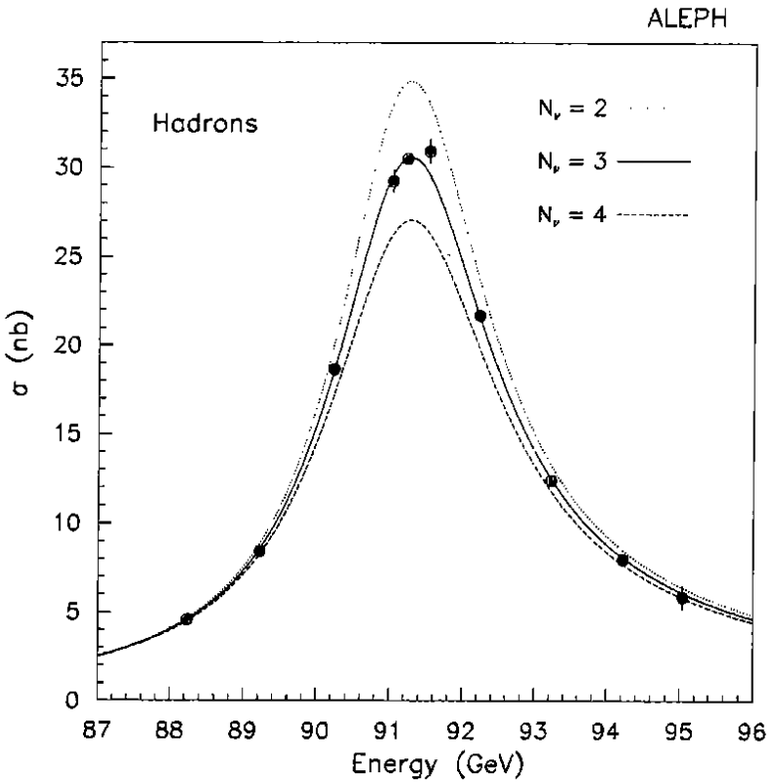

Figure 12: Cross sections for $e^+e^- \rightarrow$ hadrons as a function of the centre-of-mass energy. For points where the energy difference is less than 100 MeV the average cross section is plotted. The Standard Model predictions for $N_\nu = 2$,3, and 4 are shown.

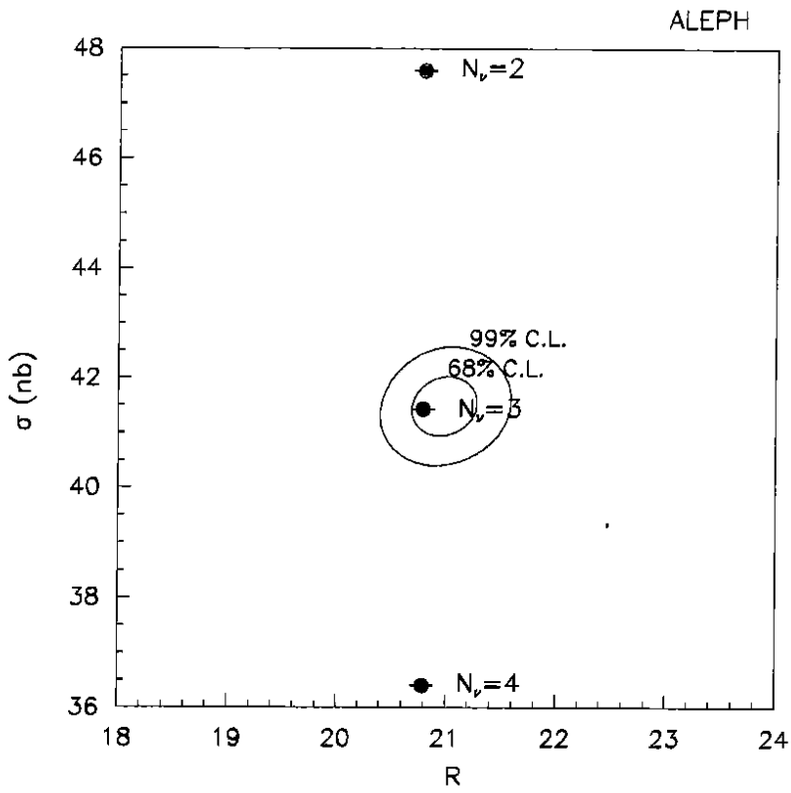

Figure 13: Contours of constant χ^2 for the hadronic peak cross section $\sigma^0_{\rm had}$ as a function of $\Gamma_{\rm had}/\Gamma_{\ell\ell}$ together with the Standard Model prediction. The uncertainty in the QCD correction is indicated by the error bar and corresponds to $\Delta\alpha_s = \pm 0.01$

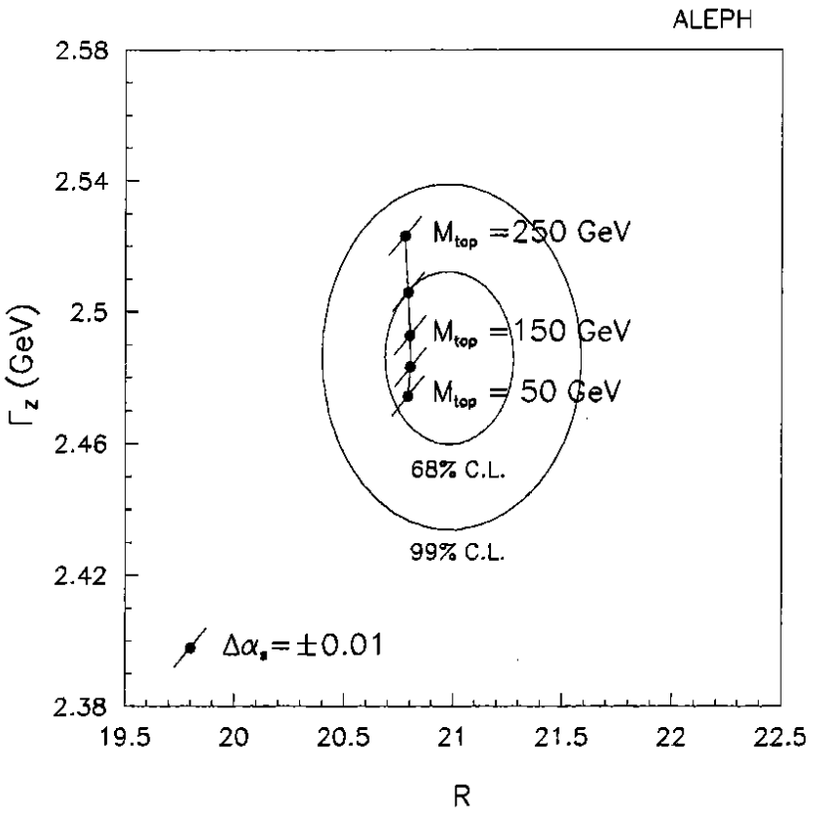

Figure 14: Contours of constant χ^2 for Γ_Z as a function of $\Gamma_{had}/\Gamma_{\ell\ell}$ together with the Standard Model predictions for various top masses (assuming $M_{Higgs} = 200$ GeV). The uncertainty resulting from the QCD correction is indicated by the error bars.

where $R^\circ = 19.98 \pm 0.03$ [20] is the Standard Model prediction for R in the absence of strong interactions.Refitting the data imposing $N_\nu = 3$, one obtains $R = R^0(1.049 \pm 0.008)$, which gives

$$\alpha_s(M_Z^2) = 0.144 \pm 0.024.$$

8.3 The Electroweak Mixing Angle and Radiative Effects

In the Standard Model, the weak vector and axial-vector couplings are defined in terms of the weak mixing angle $\sin^2\theta_W$. The measurements of the Z lineshape and the forward-backward asymmetries may be interpreted as different measurements of $\sin^2\theta_W(M_Z^2)$. The comparison of these measurements provides a fundamental test of the Standard Model and is sensitive to physics outside of the Standard Model.

The effective vector and axial vector couplings may be written as

$$g_A(M_Z^2) = -1/2\sqrt{1+\Delta\rho_\ell} \quad (6)$$

$$g_V(M_Z^2) = g_A(M_Z^2)(1-4(\sin^2\theta_W(M_Z^2)+C_\ell)). \quad (7)$$

The effective parameters $\Delta\rho_\ell$ and $\sin^2\theta_W(M_Z^2)$ [21,22,23] absorb, by definition, any deviation from the tree-level couplings not explicitly included in the fitting formula (see Appendix). $C_\ell = 0.0007$ is the flavor-dependent electroweak vertex correction [32]; $\Delta\rho_\ell$, as defined in Eq. 6 [33], includes the corresponding electroweak vertex correction to $\Delta\rho$.[7]

The lepton forward-backward asymmetry provides a direct measurement of $\sin^2\theta_W(M_Z^2)$ since it determines the ratio of vector to axial-vector coupling constants of the leptons (Eqs. 4 and 7). The measurement of the forward-backward asymmetry for leptons presented here corresponds to

$$\sin^2\theta_W(M_Z^2) = 0.2281 \pm 0.0040.$$

Other ALEPH asymmetry measurements similarly determine $\sin^2\theta_W(M_Z^2)$:

- the quark charge asymmetry [24],
- the tau polarization [11],
- the $b\bar{b}$ and $c\bar{c}$ forward-backward asymmetries [35].

The different measurements of $\sin^2\theta_W(M_Z^2)$ are summarized in Table 9, showing good agreement in the values of $\sin^2\theta_W(M_Z^2)$, with an average of

$$\sin^2\theta_W(M_Z^2) = 0.2285 \pm 0.0025.$$

[7] $\Delta\rho_\ell$ is related to $\Delta\rho$ by an electroweak vertex correction [34]:

$$\Delta\rho_\ell = \Delta\rho + C.$$

For large values of $M_{\rm top}$, the leading behaviour of $\Delta\rho$ is given by

$$\Delta\rho \simeq \frac{\alpha}{\pi}\frac{M_{\rm top}^2}{M_Z^2} - \frac{\alpha}{4\pi}\ln\frac{M_{\rm Higgs}^2}{M_Z^2}.$$

In a similar approximation, $\sin^2\theta_W(M_Z^2)$ may be written as

$$\sin^2\theta_W(M_Z^2) \simeq 1 - \frac{M_W^2}{(1+\Delta\rho)M_Z^2}.$$

Table 9: Different measurements of $\sin^2\theta_W(M_Z^2)$. $b\bar{b}$ and $c\bar{c}$ asymmetries have been combined using a 20% correlation.

Measurement	Measured quantity	value	$\sin^2\theta_W(M_Z^2)$
Lepton F-B asymmetry	$g_V^2(M_Z^2)/g_A^2(M_Z^2)$	0.0072 ± 0.0027	0.2281 ± 0.0040
Quark charge asymmetry	$< Q_{FB} >$	-0.0084 ± 0.0016	0.2300 ± 0.0052
Tau polarization	P_τ^0	-0.152 ± 0.045	0.2302 ± 0.0057
$b\bar{b}$ asymmetry	A_{FB}^b	0.126 ± 0.030	0.2262 ± 0.0054
$c\bar{c}$ asymmetry	A_{FB}^c	0.064 ± 0.049	0.2310 ± 0.0120
Asymmetry average			0.2285 ± 0.0025
Line shape	$\Gamma_{\ell\ell}$	83.05 ± 0.67 MeV	0.2340 ± 0.0025
Overall average			0.2312 ± 0.0018

The leptonic width can also be related to $\sin^2\theta_W(M_Z^2)$:

$$\Gamma_{\ell\ell} = (1+\kappa)\ \frac{\alpha(M_Z^2)\ M_Z}{48\sin^2\theta_W(M_Z^2)\cos^2\theta_W(M_Z^2)}\ \left[(1-4(\sin^2\theta_W(M_Z^2)+C_\ell))^2+1\right]\left(1+\frac{3}{4}\frac{\alpha}{\pi}\right).$$

Comparing this expression with the one obtained by substituting Eqs. 6 and 7 into Eq. 3, M_Z^2 can be related to $\sin^2\theta_W(M_Z^2)$:

$$M_Z^2 = \frac{\pi\alpha(M_Z^2)(1+\kappa)}{\sqrt{2}G_F(1+\Delta\rho_\ell)\sin^2\theta_W(M_Z^2)\cos^2\theta_W(M_Z^2)}. \tag{8}$$

The factor κ absorbs the running of the Z self-energy across the Z resonance, as well as residual vertex corrections. κ, which is related to the variable S discussed in [36] ($S = \kappa \times 4\sin^2\theta_W(M_Z^2)\cos^2\theta_W(M_Z^2)/\alpha$), depends logarithmically on both M_{top} and M_{Higgs}, and is therefore relatively more sensitive to M_{Higgs} than $\Delta\rho_\ell$. There is no explicit $\Delta\rho_\ell$ dependence in the expression for $\Gamma_{\ell\ell}$, while the $\Delta\rho_\ell$ dependence remains in the relationship between $\sin^2\theta_W(M_Z^2)$ and M_Z.

If one assumes the Minimal Standard Model value[8] of $\kappa = 0.0033 \pm 0.0010_{top} \pm 0.0015_{Higgs}$, the measurement of $\Gamma_{\ell\ell}/M_Z$ corresponds to

$$\sin^2\theta_W(M_Z^2) = 0.2340 \pm 0.0025.$$

It is interesting to note that the precision of $\sin^2\theta_W(M_Z^2)$ as determined from the asymmetry measurements is comparable to the one obtained from $\Gamma_{\ell\ell}/M_Z$ (see Table 9). The combined result is $\sin^2\theta_W(M_Z^2) = 0.2312 \pm 0.0018$.

The correlation between $\Gamma_{\ell\ell}$ and $\sin^2\theta_W(M_Z^2)$ measured from the asymmetries is shown in Fig. 15, along with the Standard Model predictions. The comparison of these measurements may also be interpreted as a measurement of κ:

$$\kappa = -0.016 \pm 0.012.$$

The agreement between this measurement of κ and its Minimal Standard Model value [20] constitutes a 1% test of the Minimal Standard Model at the 1-loop level. In nonminimal theories, κ provides a test of the Higgs sector [37]. Such a scenario is discussed in [36] where the quantity S is expected to be increased by 2.1 for one generation of technifermions in $N_c = 4$ technicolor; this change corresponds to an increase of 0.024 in κ. The measured value of κ excludes this possibility at more than a 95% confidence level (see Fig. 15).

[8]The quoted errors correspond to the M_{top} and M_{Higgs} ranges given in [20].

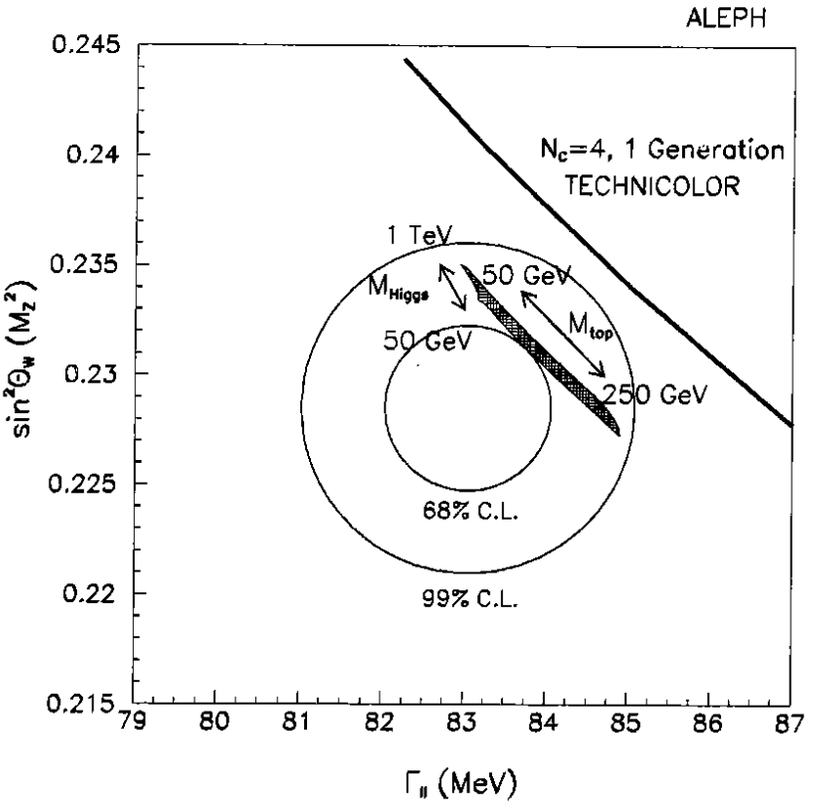

Figure 15: Contours of constant χ^2 for $\sin^2\theta_W(M_Z^2)$ from asymmetry measurements versus $\Gamma_{\ell\ell}$. The Standard Model predictions as a function of $M_{\rm top}$ and $M_{\rm Higgs}$ are shown. The expectation for one generation of technifermions in $N_c = 4$ technicolor is indicated also.

8.4 $\sin^2\theta_W(M_Z^2)$ and Limits on the Top Mass

In the Minimal Standard Model with three neutrino species, any observable can be computed as a function of $\sin^2\theta_W(M_Z^2)$, M_{top}, M_{Higgs}, and α_s. Therefore, for given values of α_s and M_{Higgs}, each observable defines a relationship between $\sin^2\theta_W(M_Z^2)$ and M_{top}. These relationships are shown in Fig. 16, assuming $\alpha_s = 0.121 \pm 0.008$ [30] and M_{Higgs}=200 GeV.[9] In addition to the constraints from the measurements presented in this paper, the constraint from the determination of the mass ratio M_W/M_Z in neutrino-nucleon scattering experiments [38] and from the direct measurement of M_W in $p\bar{p}$ colliders [39,40] is shown. The width of the band for each observable corresponds to the experimental uncertainty in the measurement. As shown in the previous section, the asymmetries depend on $\sin^2\theta_W(M_Z^2)$, but have no explicit top-mass dependence. Therefore, the constraint from the asymmetry measurements appears as a horizontal band. The other observables depend on M_{top} as well as $\sin^2\theta_W(M_Z^2)$, and appear as curved bands in Fig. 16.[10]

The data displayed in Fig. 16 may be combined to find best values of $\sin^2\theta_W(M_Z^2)$ and M_{top}. The following measurements are considered in a combined fit:

- from the lineshape:
  $M_Z = (91.182 \pm 0.009)$ GeV
  $\Gamma_Z = (2484 \pm 17)$ MeV
  $\Gamma_{had} = (1744 \pm 15)$ MeV
  $\Gamma_{\ell\ell} = (83.1 \pm 0.7)$ MeV
- from the asymmetries:
  $\sin^2\theta_W(M_Z^2) = 0.2285 \pm 0.0025$
- from measurements of the vector boson masses ratio [38,39,40]:
  $\sin^2\theta_W = 1 - \frac{M_W^2}{M_Z^2} = 0.2292 \pm 0.0042$.

A fit to the ALEPH results alone yields

$$\sin^2\theta_W(M_Z^2) = 0.2312 \pm 0.0016 \pm 0.0002_{Higgs} \quad \text{and}$$

$$M_{top} = (170 \pm^{42}_{55} \pm^{21}_{14\ Higgs}) \text{ GeV}$$

with χ^2=2.8 for 2 degrees of freedom. The second error shows the uncertainty corresponding to a change in the Higgs mass from 50 GeV [41] to 1000 GeV. These results may be interpreted as a measurement of the W boson mass:

$$M_W = (80.33^{+0.30}_{-0.32}) \text{ GeV}.$$

Combining the ALEPH results with the determination of the M_W/M_Z ratio from other experiments [39,40], one obtains a more precise determination of $\sin^2\theta_W(M_Z^2)$ and M_{top}:

$$\sin^2\theta_W(M_Z^2) = 0.2322 \pm 0.0009 \pm 0.0003_{Higgs}$$

$$M_{top} = (139 \pm^{30}_{35} \pm^{22}_{15\ Higgs}) \text{ GeV}$$

with χ^2=4.4 for 5 degrees of freedom.

[9] The theoretical calculations used include M_{top}^4 two-loop contributions as well as QCD corrections to the top mass dependent terms.

[10] Note that the constraints derived from $\Gamma_{\ell\ell}$ and M_Z are displayed separately. The constraint from the ratio $\Gamma_{\ell\ell}/M_Z$, as discussed in the previous section, would appear as a horizontal band.

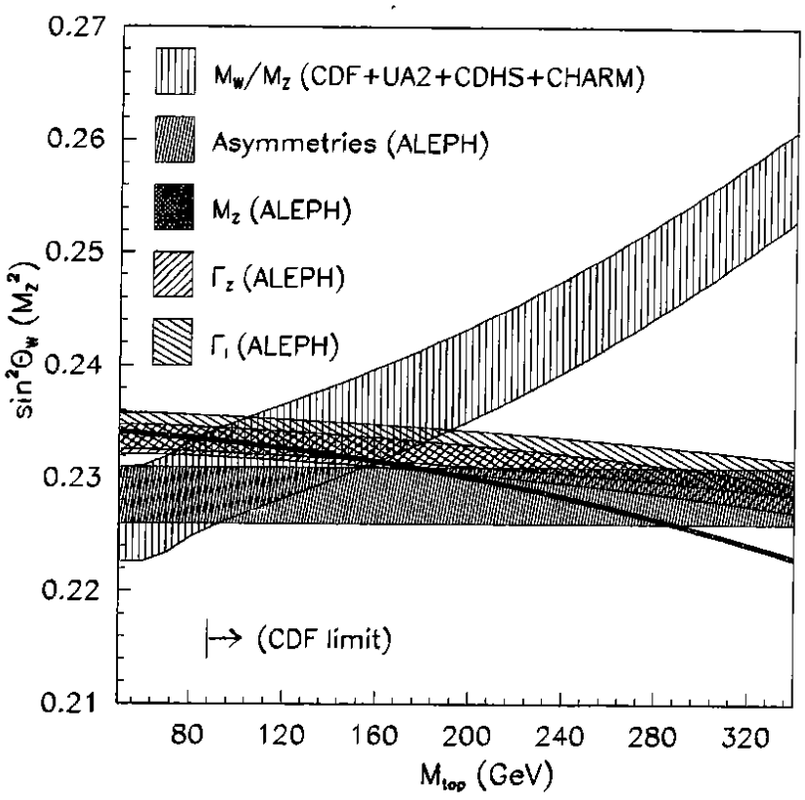

Figure 16: Constraints on $\sin^2\theta_W(M_Z^2)$ versus M_{top} from different measurements assuming $M_{Higgs} = 200$ GeV.

An independent analysis has been done in which the data are tested for consistency with the Minimal Standard Model using EXPOSTAR[21,29,42]. The only free parameters in this analysis are M_Z, M_{top}, M_{Higgs}, and α_s. Imposing $M_{Higgs} = 200$ GeV and using the ALEPH measurement of α_s [30] as a constraint, the data are found to agree with the Minimum Standard Model, and result [11] in $M_Z = (91.182 \pm 0.009)$ GeV and $M_{top} = (157^{+49}_{-71})$ GeV, consistent with the values given above.

9 Conclusion

On the basis of 190,000 Z decays collected with the ALEPH detector, the following parameters of the Z resonance have been measured:

$$\begin{aligned} M_Z &= (91.182 \pm 0.009_{exp} \pm 0.020_{LEP}) \text{ GeV} \\ \Gamma_Z &= (2484 \pm 17) \text{ MeV} \\ \sigma^0_{had} &= (41.44 \pm 0.36) \text{ nb} \\ R &= 21.00 \pm 0.20. \end{aligned}$$

The corresponding number of light neutrino species is 2.97 ± 0.07. From the forward-backward asymmetry, the ratio of vector to axial vector couplings is found to be

$$g_V(M_Z^2)^2/g_A(M_Z^2)^2 = 0.0072 \pm 0.0027.$$

[11]The quark-charge and $b\bar{b}$ asymmetry measurements have not been included in this analysis.

Using ALEPH's asymmetry measurements together with $\Gamma_{\ell\ell}/M_{\rm Z}$ yields

$$\sin^2\theta_{\rm W}(M_{\rm Z}^2) = 0.2312 \pm 0.0018.$$

A fit to the ALEPH data assuming $M_{\rm Higgs} = 200$ GeV gives

$$M_{\rm top} = (170 \pm^{42}_{55} \pm^{21}_{14\ \rm Higgs})\ \rm GeV,$$

where the second error corresponds to a change in the Higgs mass from 50 GeV to 1 TeV.

All of the results presented here are consistent with the Minimal Standard Model at a 1% level, as well as with previous measurements [1,43].

10 Acknowledgements

It is a pleasure to thank our colleagues from the SL division for the operation of LEP. We are indebted to the engineers and technicians at CERN and our home institutes for their contributions to ALEPH's success. Those of us not from member states thank CERN for its hospitality.

Appendix

In this Appendix, the parametrizations used for fitting the lineshape and forward-backward asymmetry are described. Some small contributions, such as initial-final state interference, are not easily treated in the model-independent scheme used, and have been neglected.

The cross section $\sigma_{e^+e^-\to f\overline{f}}$ can be expressed in a model-independent way in terms of three contributions:

- the Z exchange that is represented by a Breit-Wigner function;
- the photon exchange;
- the Z-γ interference term I_f.

The following expression is used for the fits:

$$\begin{aligned}\sigma(s)_{ff} &= \frac{s}{(s-M_Z^2)^2+s^2\Gamma_Z^2/M_Z^2}\left(\frac{12\pi\Gamma_{ff}}{M_Z^2}\frac{\Gamma_{ee}}{1+\frac{3}{4}\frac{\alpha}{\pi}}+I_f\frac{N_c(s-M_Z^2)}{s}\right)\\ &+\frac{4}{3}\pi N_c Q_f^2\,\frac{\alpha^2(s)}{s},\end{aligned} \tag{9}$$

where Γ_{ee}, Γ_{ff} are the partial widths for Z decay into e^+e^- or any fermion pair $f\overline{f}$; Q_f is the charge and N_c is the colour factor of the fermion. Γ_Z is the total width and M_Z the mass of the Z boson. The invisible width is defined by $\Gamma_{\rm inv}=\Gamma_Z-\Gamma_{\rm had}-\Gamma_{ee}-\Gamma_{\mu\mu}-\Gamma_{\tau\tau}$, where $\Gamma_{\rm had}$ denotes the hadronic decay width. In this formula, Γ_{ee} is divided by the factor $(1+\frac{3}{4}\frac{\alpha}{\pi})$ to allow for a separate treatment of the initial state radiation [19], as described below. Initial state real and virtual pair production has been studied but is not yet taken into account.

The interference term, I_f, cannot be expressed in a model-independent way in terms of the Z partial widths. Since I_f is small, the Standard Model value is assumed.

To include the effect of initial-state radiation, the expression for the cross section is convoluted with a radiator function [17,44].

The QED-corrected forward-backward asymmetry in the angular distribution can be well approximated as [45]:

$$A_{\rm FB}(s)=\frac{\int_0^{x_{max}}H(s,x)\sigma_{NR}^{FB}(s(1-x))\,dx}{\int_0^{x_{max}}H(s,x)\sigma_{NR}(s(1-x))\,dx},$$

where $H(s,x)$ is the same radiator function used in the total cross section. In the numerator, $\sigma_{NR}^{FB}=\sigma_{NR}^{F}-\sigma_{NR}^{B}$ is the integrated forward minus backward non-radiatively-corrected cross section, which in terms of the effective coupling constants $g_{\rm A}(M_Z^2)$ and $g_{\rm V}(M_Z^2)$ is

$$\begin{aligned}\sigma_{NR}^{FB}(s)=\frac{\pi\alpha^2(s)}{s}\,(\quad & 2\quad g_{\rm Ae}g_{\rm Af}\,F_G(s)\,\frac{s(s-M_Z^2)+s^2\frac{\Gamma_Z}{M_Z}{\rm Im}(\Delta\alpha)}{(s-M_Z^2)^2+s^2\frac{\Gamma_Z^2}{M_Z^2}}\\ &+4\quad g_{\rm Ve}g_{\rm Ae}g_{\rm Vf}g_{\rm Af}\,F_G^2(s)\,\frac{s^2}{(s-M_Z^2)^2+s^2\frac{\Gamma_Z^2}{M_Z^2}}\;),\end{aligned}$$

where ${\rm Im}(\Delta\alpha)$ is the imaginary part of the photon vacuum polarization. The denominator is the total cross section, which can be expressed as

$$\sigma_{NR}(s) = \frac{4}{3}\,\frac{\pi\alpha^2(s)}{s}\,\Big(\;1\;+\;2\;g_{\rm Ve}g_{\rm Vf}\,F_G(s)\,\frac{s(s-M_{\rm Z}^2)}{(s-M_{\rm Z}^2)^2+s^2\frac{\Gamma_{\rm Z}^2}{M_{\rm Z}^2}}+$$

$$((g_{\rm Ve})^2+(g_{\rm Ae})^2)\;\cdot\;((g_{\rm Vf})^2+(g_{\rm Af})^2)\;F_G^2(s)\,\frac{s^2}{(s-M_{\rm Z}^2)^2+s^2\frac{\Gamma_{\rm Z}^2}{M_{\rm Z}^2}}\;\Big),$$

where

$$F_G = \frac{G_F M_{\rm Z}^2}{2\sqrt{2}\pi\alpha(s))}. \tag{10}$$

The parametrizations used for the lineshape and the forward-backward asymmetry are good approximations of the most accurate Standard-Model calculations available.

References

[1] D. Decamp *et al.* (ALEPH Coll.): Z. Phys. C 48 (1990) 365 (1990).

[2] D. Decamp *et al.* (ALEPH Coll.): Nucl. Instr. Methods A294 (1990) 121.

[3] D. Decamp *et al.* (ALEPH Coll.):"Measurement of the Absolute Luminosity with the ALEPH detector," to be submitted to Z. Phys. C.

[4] W. Beenakker, F.A. Berends, and S.C. van der Marck: Nucl. Phys. B349 (1991) 323.

[5] M. Martinez and R. Miquel: "Fitting the $e^+e^- \rightarrow e^+e^-$ Lineshape", CERN-PPE 91-87, submitted to Z. Phys. C.

[6] S. Jadach and Z. Wąs: Phys. Rev. D41 (1990) 1425.

[7] F.A. Berends and R. Kleiss: Nucl. Phys. B228 (1983) 737,
M. Böhm, A. Denner and W. Hollik: Nucl. Phys. B304 (1988) 687,
F.A. Berends, R. Kleiss and W. Hollik: Nucl. Phys. B304 (1988) 712, and
Computer program BABAMC, courtesy of R. Kleiss.

[8] S. Jadach and Z. Wąs: Comp. Phys. Commun. 36 (1985) 191; and Monte Carlo Group in "Proceedings of the Workshop on Z Physics at LEP," CERN Report 89-08 (1989) Vol. III;
S. Jadach, B.F.L. Ward and Z. Wąs: CERN-TH 961-90, to be published in Comp. Phys. Commun. Computer program KORALZ, courtesy of S. Jadach, B.F.L. Ward and Z. Wąs.

[9] M. Bengtsson, T. Sjostrand: Phys. Lett. B185 (1987) 435; G. Marchesini, B.R. Weber: Nucl. Phys. B310 (1988) 461.

[10] S. Kawabata: Comp. Phys. Comm. 41 (1986) 127.

[11] D. Decamp *et al.*(ALEPH Coll.): "Measurement of the Polarization of τ Leptons Produced in Z Decays," CERN-PPE 91-94, submitted to Phys. Lett. B.

[12] S. Jadach, E. Richter-Wąs, Z. Wąs and B.F.L. Ward: Phy. Lett. B260 (1991) 438.

[13] W. Beenakker, F.A. Berends, and S.C. van der Marck: Nucl. Phys. B355 (1991) 281.

[14] V. Hatton *et al.*: "LEP Absolute Energy in 1990," LEP Performance R. Baily *et al.*: "LEP Energy Calibration," CERN-SL 90-95 J.M. Jowett: "Luminosity and Energy Spread in LEP," CERN-LEP-TH 85-04 and private communication for updated values.

[15] A. Borelli *et al.*: Nucl. Phys. B333 (1990) 357.

[16] F.A. Berends *et al.*: Z Line Shape group in "Proceedings of the Workshop of Z Physics at LEP," CERN Report 89-08 Vol. I, 89.

[17] F.A. Berends, G. Burgers and W.L. van Neerven: Nucl. Phys. B297 (1988) 429 and Nucl. Phys. B304 (1988) 921.

[18] D. Bardin *et al.*: Z. Phys. C44 (1989) 493.

[19] M. Martinez, L. Garrido, R. Miquel, J.L. Harton ,R. Tanaka: Z. Phys. C49 (1991) 645.

[20] The Standard model predictions correspond to the following values: $M_{\rm top} = (130^{+120}_{-50})$ GeV, $M_{\rm Higgs} = (200^{+800}_{-150})$ GeV, and $\alpha_s = 0.12 \pm 0.01$.

[21] D.C. Kennedy and B.W. Lynn: Nucl. Phys. B322 (1989) 1.

[22] M. Consoli and W. Hollik: in in "Proceedings of the Workshop of Z Physics at LEP," CERN Report 89-08 Vol. I, 7.

[23] W.J. Marciano and A. Sirlin: Phys. Rev. Lett. 46 (1981) 163.

[24] D. Decamp *et al.*(ALEPH Coll.): Phys. Lett. B259 (1991) 377.

[25] K. Abe *et al.*: Phys. Rev. Lett. 62 (1989)1709.

[26] D. Geiregat *et al.*(CHARM II Coll.): Phys. Lett. B259 (1991) 499.

[27] J. Dorenbosch *et al.*(CHARM Coll.): Z. Phys. C41 (1989) 567.

[28] R.C. Allen *et al.*: Phys. Rev. Lett. 64 (1990) 1330.

[29] D.C. Kennedy, B.W. Lynn, C.J.-C. Im, and R.G. Stuart: Nucl. Phys. 321B 83 (1989);
B. W. Lynn, S. Selypsky, R.G. Stuart, D. Levinthal, in preparation.

[30] D. Decamp *et al.*(ALEPH Coll.): Phys. Lett. B255 (1990) 623; D. Decamp *et al.*(ALEPH Coll.): Phys. Lett. B257 (1991) 479.

[31] K.G. Cheterkyn, A.L. Kateev and F.V. Tkachov: Phys. Lett. B85 (1979) 277;
M. Dine and J. Sarpinstein: Phys. Rev. Lett. 43 (1979) 668;
W. Celemaster and R.J. Gonsalves: Phys. Rev. Lett. 44 (1979) 560 and Phys. Rev. D21 (1980) 3112.

[32] D. Bardin, W. Hollik, and T. Riemann: Z. Phys. C 49 (1991) 485.

[33] This definition of $\Delta\rho_\ell$ follows the suggestion of G. Altarelli and R. Barbieri: Phys. Lett. B230 (1991) 161.

[34] W. Hollik: private communication.

[35] D. Decamp *et al.*(ALEPH Coll.): "Measurement of the Forward-Backward Asymmetry in $Z \to b\bar{b}$ and $Z \to c\bar{c}$," CERN-PPE 91-71, submitted to Phys. Lett. B.

[36] M. E. Peskin and T. Takeuchi: Phys. Rev. Lett. 65 (1990) 964.

[37] B.W. Lynn, M.E. Peskin, and R.G. Stuart: in "Physics at LEP," CERN Report 86-02 Vol. I, 90.

[38] H. Abramowicz *et al.*(CDHS Coll.): Phys. Rev. Lett. 57 (1986) 298, and
A. Blondel *et al.*: Z. Phys. C45 (1990) 361.
J.V. Allaby *et al.*(CHARM Coll.): Phys. Lett B177 (1986) 446, and Z. Phys. C36 (1987) 611.

[39] J. Alitti *et al.*(UA2 Coll.): Phys. Lett. B241 (1990) 150.

[40] F. Abe *et al.*(CDF Coll.): Phys. Rev. Lett. 65 (1990) 2243.

[41] D.Decamp, *et al.*(ALEPH Coll.) : "Searches for the Standard Higgs Boson Produced in the Reaction $e^+e^- \to H^0Z^*$," CERN-PPE 91-19.

[42] D. Levinthal, F. Bird, R. G. Stuart, and B. W. Lynn: CERN-TH 6094/91 submitted to Z. Phys. C.

[43] P. Abreu *et al.*(DELPHI Coll.): "Determination of the Z^0 Resonance Parameters and Couplings from its Hadronic and Leptonic Decays," CERN-PPE 91-95;
B. Adeva *et al.*(L3 Coll.): "Measurement of Electroweak Parameters from Hadronic and Leptonic Decays of the Z^0," L3 Preprint 28 (1991);
G. Alexander *et al.*(OPAL Coll.): "Measurement of the Z^0 Line Shape Parameters and the Electroweak Coupling of Charged Leptons," CERN-PPE 91-67, submitted to Z. Phys. C.

[44] E.A. Kuraev, V.S. Fadin: Sov. J. Nucl. Phys. 41 (1985) 466,
G. Altarelli, G. Martinelli: in "Physics at LEP," CERN 86-02 (1986) Vol. I,47,
O. Nicrosini, L. Trentadue: Phys. Lett. B196 (1987) 551.

[45] D. Bardin *et al.*: in Proceedings of the Workshop of Z Physics at LEP, CERN Report 89-08, 1989, Vol. I, 203.